



# Comprehensive mapping and characteristic regimes of aerosol effects on the formation and evolution of pyro-convective clouds

D. Chang<sup>1</sup>, Y. Cheng<sup>1</sup>, P. Reutter<sup>2</sup>, J. Trentmann<sup>3</sup>, S. M. Burrows<sup>4</sup>, P. Spichtinger<sup>2</sup>, S. Nordmann<sup>1</sup>, M. O. Andreae<sup>5</sup>, U. Pöschl<sup>1</sup>, and H. Su<sup>1</sup>

<sup>1</sup>Multiphase Chemistry Department, Max Planck Institute for Chemistry, Mainz, Germany

<sup>2</sup>Institute for Atmospheric Physics (IPA), Johannes Gutenberg University Mainz, Mainz, Germany

<sup>3</sup>German Weather Service (DWD), Offenbach, Germany

<sup>4</sup>Pacific Northwest National Laboratory, Richland, WA, USA

<sup>5</sup>Biogeochemistry Department, Max Planck Institute for Chemistry, Mainz, Germany

Correspondence to: H. Su (h.su@mpic.de)

Received: 29 January 2014 – Published in Atmos. Chem. Phys. Discuss.: 21 March 2014

Revised: 22 June 2015 – Accepted: 11 August 2015 – Published: 21 September 2015

**Abstract.** A recent parcel model study (Reutter et al., 2009) showed three deterministic regimes of initial cloud droplet formation, characterized by different ratios of aerosol concentrations ( $N_{CN}$ ) to updraft velocities. This analysis, however, did not reveal how these regimes evolve during the subsequent cloud development. To address this issue, we employed the Active Tracer High Resolution Atmospheric Model (ATHAM) with full microphysics and extended the model simulation from the cloud base to the entire column of a single pyro-convective mixed-phase cloud. A series of 2-D simulations (over 1000) were performed over a wide range of  $N_{CN}$  and dynamic conditions. The integrated concentration of hydrometeors over the full spatial and temporal scales was used to evaluate the aerosol and dynamic effects. The results show the following. (1) The three regimes for cloud condensation nuclei (CCN) activation in the parcel model (namely aerosol-limited, updraft-limited, and transitional regimes) still exist within our simulations, but net production of raindrops and frozen particles occurs mostly within the updraft-limited regime. (2) Generally, elevated aerosols enhance the formation of cloud droplets and frozen particles. The response of raindrops and precipitation to aerosols is more complex and can be either positive or negative as a function of aerosol concentrations. The most negative effect was found for values of  $N_{CN}$  of  $\sim 1000$  to  $3000\text{ cm}^{-3}$ . (3) The nonlinear properties of aerosol–cloud interactions challenge the conclusions drawn from limited case studies in terms of their representativeness, and ensemble

studies over a wide range of aerosol concentrations and other influencing factors are strongly recommended for a more robust assessment of the aerosol effects.

## 1 Introduction

Clouds have a considerable impact on the radiation budget and water cycle of the Earth (IPCC, 2007). Aerosol effects on clouds and precipitation have been suggested to influence the formation, persistence, and ultimate dissipation of clouds and its climate effects (Stevens and Feingold, 2009; Tao et al., 2012) and hence have been studied intensively through cloud-resolving model simulations, analysis of satellite data, and long-term observational data (Tao et al., 2012).

However, aerosol effects are still associated with significant uncertainty in light of the seemingly contradictory results from different studies. For instance, several studies have indicated that increasing aerosol concentrations could reduce cloud fraction and inhibit cloud formation (Albrecht, 1989; Ackerman et al., 2000; Kaufman et al., 2002; Koren et al., 2004), whereas it is suggested that more aerosols can increase the cloud fraction in other studies (Norris, 2001; Kaufman and Koren, 2006; Grandey et al., 2013). Precipitation from stratiform clouds can be inhibited by elevated aerosol concentration (Zhang et al., 2006), while precipitation from convective clouds can be either suppressed or enhanced (Ackerman et al., 2003; Andreae et al., 2004; Altartaz

et al., 2008; Lee et al., 2008; Teller and Levin, 2008; Fan et al., 2013; Camponogara et al., 2014). In addition, changing aerosol concentrations have also been found to exert non-monotonic influences (either positive or negative) on a wide range of cloud properties, such as homogeneous freezing (Kay and Wood, 2008), frozen water particles (Saleeby et al., 2009; Seifert et al., 2012), and convection strength (Fan et al., 2009).

One explanation for these seemingly contradictory results is that aerosol effects are regime-dependent, which means that aerosol effects can vary under different meteorological conditions (updraft velocity, relative humidity, surface temperature, and wind shear), cloud types, aerosol properties (size distribution and chemical composition), and observational or analysis scales (Levin and Cotton, 2007; Tao et al., 2007; Khain et al., 2008; Rosenfeld et al., 2008; Fan et al., 2009; Khain, 2009; Reutter et al., 2009; McComiskey and Feingold, 2012; Tao et al., 2012). It is thus important to investigate the regime dependence of aerosol–cloud interactions and to improve the representation of cloud regimes in models (Stevens and Feingold, 2009). Being able to distinguish those conditions under which cloud formation is updraft-limited (aerosol-insensitive) as discussed in Reutter et al. (2009) would provide the advantage for future work that one could, for many purposes, neglect aerosol effects on clouds in areas that are usually updraft-limited.

Another challenge in evaluating the aerosol effects lies in the nonlinear properties of aerosol–cloud interactions. Most previous research has investigated the response of clouds and precipitation to the perturbation of aerosols based on two or several individual scenarios by doubling or tripling the number concentration of aerosol particles. This is will be fine for the linear dependence. Since aerosol–cloud interaction is a nonlinear process, such a method may not reflect the real aerosol effect. An exemplary case is shown in Fig. 1, in which it is clear that the local derivatives ( $dY/dX$ ) can be different from  $\Delta Y/\Delta X$  determined by the difference between A and B cases.

Biomass burning generates significant amounts of smoke aerosols, and the fires loft soil particles that contain minerals (Pruppacher and Klett, 1997); both of these aerosol particles could serve as effective cloud condensation nuclei (CCN) and ice nuclei (IN) (Hobbs and Locatelli, 1969; Hobbs and Radke, 1969; Kaufman and Fraser, 1997; Sassen and Khvorostyanov, 2008), thereby affecting the formation of clouds and precipitation. As an extreme consequence of biomass burning, pyro-clouds feed directly from the smoke and heat released from fires (Andreae et al., 2004; Luderer, 2007) and provide a good example with which to study aerosol–cloud interactions (Reutter et al., 2009).

By taking the pyro-convective clouds as an example, here we demonstrate the ability of ensemble simulations to determine the regime dependence and resolve the nonlinear properties of aerosol–cloud interactions. Aerosol number concentration, updraft velocity (represented by the intensity of fire

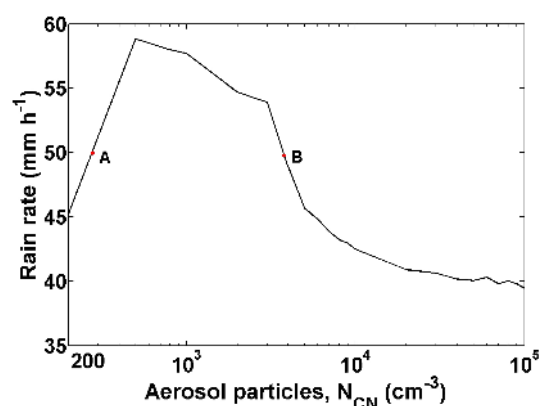


**Figure 1.** Conceptual model of the nonlinear relationship between aerosol concentrations and rain rate (data are from 2-D simulation results of this work).

forcing, which triggers updraft velocities), and key parameters of CCN activation (Reutter et al., 2009) are varied to represent a wide range of aerosol and dynamic conditions. In addition to cloud droplets, the responses of precipitable hydrometeors (raindrops, ice, snow, graupel, and hail) were also investigated. For a better understanding of the mechanisms, we employed the process analysis (PA) method, which documents the rate of change in the mass or number concentration of each hydrometeor type caused by a particular process, thereby enabling the determination of the relative importance of the major microphysical processes under different dynamic forcing and aerosol conditions.

## 2 Design of numerical experiments

### 2.1 ATHAM: model and configuration

The Active Tracer High Resolution Atmospheric Model (ATHAM), a non-hydrostatic model, is used here to study cloud formation and evolution in response to changes in updrafts and aerosol particle concentration. ATHAM was designed initially to investigate high-energy plumes in the atmosphere and applied to simulate volcanic eruptions and fire plumes (Herzog, 1998; Oberhuber et al., 1998). ATHAM has been used to simulate the evolution of pyro-cumulonimbus clouds (pyroCb) caused by a forest fire and shows results consistent with observations (Luderer, 2007).

The model comprises eight modules: dynamics, turbulence, cloud microphysics, ash aggregation, gas scavenging, radiation, chemistry, and soil modules (Herzog et al., 1998, 2003; Oberhuber et al., 1998; Graf et al., 1999). Cloud microphysical interactions are represented by an extended version of the two-moment scheme developed by Seifert and Beheng (2006), which includes the hail modifications by Blahak (2008) and is able to predict the numbers and mass mixing ratios of six classes of hydrometeors (cloud water, ice crystals,

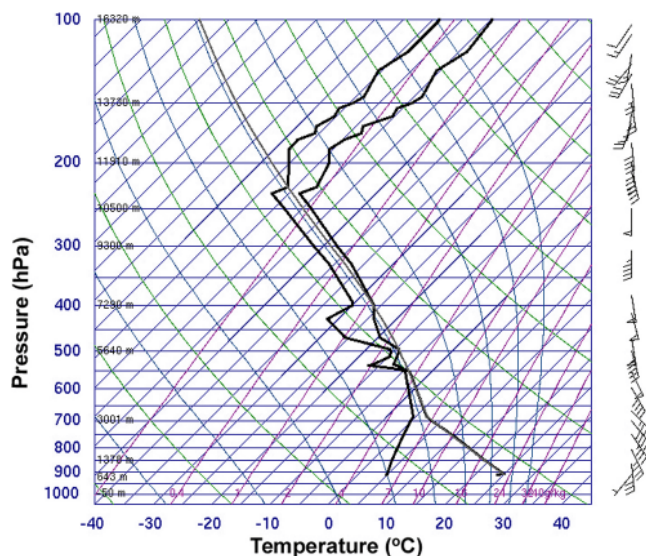


**Figure 2.** Atmospheric sounding launched near Edmonton, Alberta, on 29 May 2001. The right black line represents the temperature, and the left black line corresponds to the dew-point temperature. This weather information is from the University of Wyoming Department of Atmospheric Science (<http://weather.uwyo.edu/s>).

raindrops, snow, graupel, and hail; detailed in Table 1) and water vapor. It has been validated successfully against a comprehensive spectral bin microphysics cloud model (Seifert et al., 2006). The cloud nucleation (CCN activation) module is based on a lookup table derived from parcel model simulations for pyro-convective clouds (Reutter et al., 2009). ATHAM can execute both 2-D and 3-D simulations. Results of this study are mainly based on 2-D simulations.

The meteorological conditions were set up to simulate the Chisholm forest fire (Luderer, 2007; Rosenfeld et al., 2007), which is a well-documented case of pyro-convection. All simulations were initialized horizontally homogeneously with radiosonde data from about 200 km south of the fire on 29 May 2001, which is the same as in Luderer (2007) (Fig. 2). The vertical profiles of the temperature and dew-point temperature reveal a moderate instability in the atmosphere. Open lateral boundaries were used for the model simulations. The means of wind speed and specific humidity were nudged towards the initial profile at the lateral boundaries. The fire forcing was introduced in the middle grid in the bottom layer of the domain, and its intensity remained constant throughout the simulation of each scenario. Each case was run for three simulated hours until the clouds were fully developed and had reached steady state.

The 2-D simulations were performed at the cross section of the fire front. The simulation domain was set at  $85 \times 26$  km with  $110 \times 100$  grid boxes in the  $x$  and  $z$  directions. The horizontal grid box size at the center of the  $x$  direction was equal to 500 m, and it enlarged towards the lateral boundaries due to the stretched grid (Fig. 3). Such a pro-

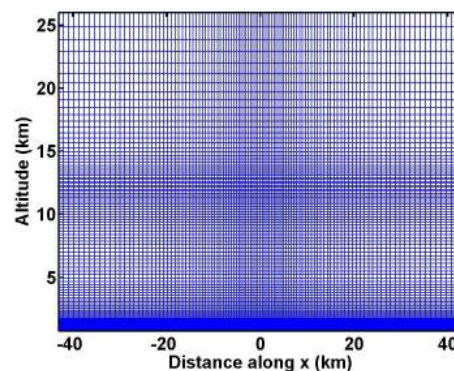


**Figure 3.** The  $110 \times 100$  grid points in the computational domain.

cess scale with resolution of ca. 1 km has been suggested as the appropriate scale at which to characterize processes related to aerosol–cloud interactions (McComiskey and Feingold, 2012). The vertical grid spacing at the surface and the tropopause was set to 50 and 150 m, respectively. The lowest vertical level in our simulation was set at 766 m above sea level, corresponding to the lowest elevation of the radiosonde data, which is close to the elevation of Chisholm at about 600 m (ASRD, 2001). The results of the 2-D simulations are presented and discussed in Sect. 3.

## 2.2 Aerosol particles and fire forcing

Atmospheric aerosol particles affect cloud formation through two pathways by acting as CCN and as IN. Following the previous study of Reutter et al. (2009), we limited the scope of aerosol–cloud interactions to CCN activation only. Thus, in this study, changes in  $N_{\text{CN}}$  do not directly influence frozen hydrometeors by providing IN; rather, they indirectly influence them through their impact on CCN activation and subsequent processes.

In the 2-D ensemble simulations, 1302 cases ( $31 N_{\text{CN}} \times 42$  fire forcing values) were simulated to evaluate the interplay of aerosol concentration and updrafts on the formation of clouds and precipitation. The  $N_{\text{CN}}$  varied from 200 to  $100\,000 \text{ cm}^{-3}$ . In each case,  $N_{\text{CN}}$  was prescribed (distributed uniformly across the modeling domain and kept identical throughout the simulation). A similar prescribed approach has been used in previous studies (Seifert et al., 2012; Reutter et al., 2014). Some previous studies have pointed out that a prescribed aerosol scheme overestimates the magnitude of CCN concentrations compared to a prognostic aerosol scheme because it lacks a representation of the efficient removal of particles by nucleation scavenging (Wang et al., 2013).

As mentioned above, we used the lookup table of Reutter et al. (2009) for the CCN activation. This table is determined for fresh biomass burning aerosols with a hygroscopicity parameter  $\kappa$  of 0.2 and a log-normal size distribution (a geometric mean diameter of 120 nm and a geometric standard

**Table 1.** Typical characterizations of the frozen hydrometeor classes.

		Diameter (mm)	Density ( $\text{g cm}^{-3}$ )	Terminal velocity ( $\text{m s}^{-1}$ )
Cloud ice	Columnar crystals	0.01–1 <sup>(1)</sup>	0.36–0.7 <sup>(2)</sup>	0.013–0.055 <sup>(2)</sup>
	Plate-like	0.01–1 <sup>(1)</sup>	$\sim 0.9$ <sup>(1)</sup>	0.02–0.06 <sup>(2)</sup>
	Dendrites	0.1–3 <sup>(1)</sup>	0.3–1.4 <sup>(1)</sup>	0.25–0.7 <sup>(3)</sup>
Snowflakes		2–5 <sup>(1)</sup>	0.05–0.89 <sup>(1)</sup>	0.5–3 <sup>(1)</sup>
Graupel		0.5–5 <sup>(1)</sup>	$\sim 0.4$ <sup>(1)</sup>	3–14 <sup>(1)</sup>
Hail		5–80 <sup>(1)</sup>	0.8–0.9 <sup>(1)</sup>	10–40 <sup>(1)</sup>

<sup>(1)</sup> Pruppacher and Klett (1997).

<sup>(2)</sup> Jayaweera and Ryan (1972).

<sup>(3)</sup> Mitchell and Heymsfield (2005).

deviation of 1.5; Reutter et al. 2009). For the present study, the aerosol characteristics, such as size distribution, chemical composition, hygroscopicity and mixing state, are in fact rather unimportant compared with the order-of-magnitude changes in the aerosol number concentration (Reutter et al., 2009; Karydis et al., 2012). Therefore, the effects of variations in aerosol characteristics were not considered in our study.

In all simulations, clouds were triggered by the fire forcing, which was assumed constant during the simulation. The fire forcing intensity varied from  $1 \times 10^3$  to  $3 \times 10^5 \text{ W m}^{-2}$ . The correlation between the initial fire forcing and corresponding updraft velocity and temperature at the cloud base was probed and is described in Sect. 3.1.

In reality, the composition and quantity of biomass burning emissions depend on the moisture content of fuels, combustion conditions, weather situation, and fire behavior (Bytnerowicz et al., 2009). Furthermore, the biomass burning plumes can in turn change the relative humidity as well. The aerosol particle number concentrations in biomass burning plumes usually exceed  $10^4 \text{ cm}^{-3}$ , and can be up to  $\sim 10^5 \text{ cm}^{-3}$  (Andreae et al., 2004; Reid et al., 2005). In contrast to regular convection, the updraft velocities in pyro-convective clouds are normally larger than 20–30  $\text{m s}^{-1}$  (Khain et al., 2005). On the basis of these facts, within our work more attention is paid to situations with higher aerosol concentration ( $> 10^4 \text{ cm}^{-3}$ ) and strong updrafts ( $> 20 \text{ m s}^{-1}$ ), which are more representative of pyro-convective clouds.

### 2.3 Process analysis

Cloud properties are subject to several tens of microphysical processes, e.g., cloud droplet nucleation, autoconversion, freezing, condensation, and evaporation (Seifert and Beheng, 2006). Elevated concentrations of hydrometeors can be caused either by an increase in their sources or by a decrease in their sinks. To improve the understanding of the aerosol–cloud interactions, we employed the process analy-

sis (PA) method to quantify the causation of changes in the concentrations of individual hydrometeor classes.

In addition to the standard model output (e.g., time and spatial series of mass and number concentrations of hydrometeors, and meteorological output), our PA method archives additional parameters, i.e., the time rate of change in hydrometeors due to individual microphysical processes under different aerosol and fire forcing conditions. Table A1 in the Appendix summarizes all the microphysical processes and their abbreviations.

### 2.4 3-D simulations

In addition, we performed a number of 3-D simulations to investigate their difference to 2-D simulations. As the 3-D simulations are computationally expensive, only 99 cases (11  $N_{\text{CN}} \times 9$  fire forcing values) were performed.  $N_{\text{CN}}$  varied from 200 to 100 000  $\text{cm}^{-3}$ , while fire forcing varied between  $1 \times 10^3$  and  $8 \times 10^4 \text{ W m}^{-2}$ . The size of the model domain was set at  $85 \times 65 \times 26 \text{ km}$  with  $110 \times 85 \times 100$  grid boxes in the  $x$ ,  $y$ , and  $z$  directions. For consistency, the grid resolutions in the  $x$  and  $z$  directions were the same as for 2-D simulations. The minimum grid box size in the  $y$  direction was set to 100 m. The results of the 3-D simulations are presented and discussed in the Supplement.

## 3 Results and discussion

### 3.1 Relationship between updraft velocity, temperature, and fire forcing

Fire forcing does not affect the cloud activation of aerosols directly, but it can affect activation indirectly by triggering strong updraft velocities. Updrafts are of importance in the formation of clouds and precipitation for redistributing energy and moisture. To cover a wide range of conditions, the updraft velocities range from ca. 0.25 to 20  $\text{m s}^{-1}$  in previous cloud parcel model simulations (Reutter et al., 2009), which

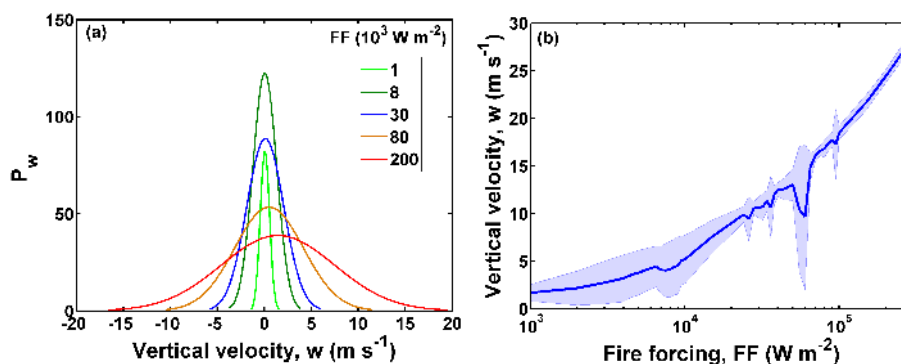


**Figure 4.** Probability distribution function of vertical velocities ( $w$ ) at cloud base layer under different fire forcing conditions (a). Relationship between input fire forcing (FF) and induced vertical velocity ( $w$ ) at cloud base (b). The aerosol concentration is  $1000 \text{ cm}^{-3}$ . The shaded area represents the variability of estimation ( $\pm 0.5\sigma$ ).

represent the range found in trade wind cumulus to thunderstorms (Pruppacher and Klett, 1997).

The probability distribution function of vertical velocities ( $w$ ) at cloud base layer under different fire forcing conditions is shown in Fig. 4a. The velocity on top of the input fire forcing is usually the largest, and decreases towards the lateral sides. These largest velocities under different fire forcing conditions, are plotted against the input fire forcing (range of  $1 \times 10^3$  to  $3 \times 10^5 \text{ W m}^{-2}$ ,  $N_{\text{CN}} = 1 \times 10^3 \text{ cm}^{-3}$ ) in Fig. 4b. The shaded area indicates the variability of estimation over each simulation period. According to the figure,  $w$  at cloud base varies monotonically from 1.8 to  $27 \text{ m s}^{-1}$  as fire forcing increases from  $1 \times 10^3$  to  $3 \times 10^5 \text{ W m}^{-2}$ . The positive relationship suggests that fire forcing could be a good indicator of vertical velocity. Because it is a variable of central interest to the cloud research community, the maximum vertical velocity is provided along with the fire forcing values as an additional axis in the following plots.

Another variable of key meteorological interest is the maximum temperature at cloud base. To clarify how temperature is affected by fire forcing in our simulations, the relationship between fire forcing and the corresponding maximum temperature at cloud base is shown in Fig. 5. As variations in aerosol number concentrations have very little effect on the temperature profile, we show this relationship for only one aerosol concentration ( $N_{\text{CN}} = 5000 \text{ cm}^{-3}$ ) as an example. As can be seen in Fig. 5, the cloud base temperature increases linearly from 7.6 to  $16.4 \text{ }^\circ\text{C}$ , as fire forcing is enhanced from  $1 \times 10^3$  to  $3 \times 10^5 \text{ W m}^{-2}$ . In order to more clearly convey the effect of the heating imposed in the simulation, we have used this linear relationship to add the maximum cloud base temperature as a secondary axis in the following figures.

Finally, we note that the horizontal wind shear can also affect the convection strength (Fan et al., 2009), which could be investigated in detail in future studies.

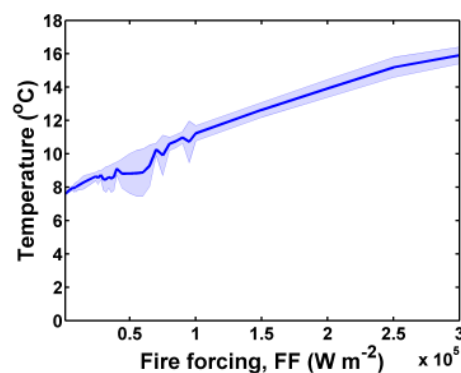


**Figure 5.** The correlation of fire forcing and the corresponding maximum temperature at cloud base. The shaded area indicates the variability of estimation ( $\pm 0.5\sigma$ ) over each simulation period.

## 3.2 Aerosol effects and its regime dependence

In this section, the spatiotemporal distribution of each hydrometeor type will be briefly presented, followed by the modeled dependency of various hydrometeors on  $N_{\text{CN}}$  and fire forcing (FF). Note here that only the characteristics of dependency are presented, while the underlying mechanisms will be discussed and interpreted in more detail in Sect. 3.3. For an individual hydrometeor type, the averaged concentrations (over the entire domain and simulation period) were used as metrics in our evaluation, and the condensed water reaching the surface was used as a metric for precipitation.

### 3.2.1 Cloud droplets

Figure 6 shows the temporal evolution of horizontally averaged mass concentration of cloud droplets ( $M_{\text{CD}}$ ) under the four pairs of FF and  $N_{\text{CN}}$  conditions. Under weak fire forcing conditions (LU), the formation of cloud droplets usually occurs after 20 min and most of cloud droplets locate in an altitude of 4–7 km. The duration of cloud droplets is

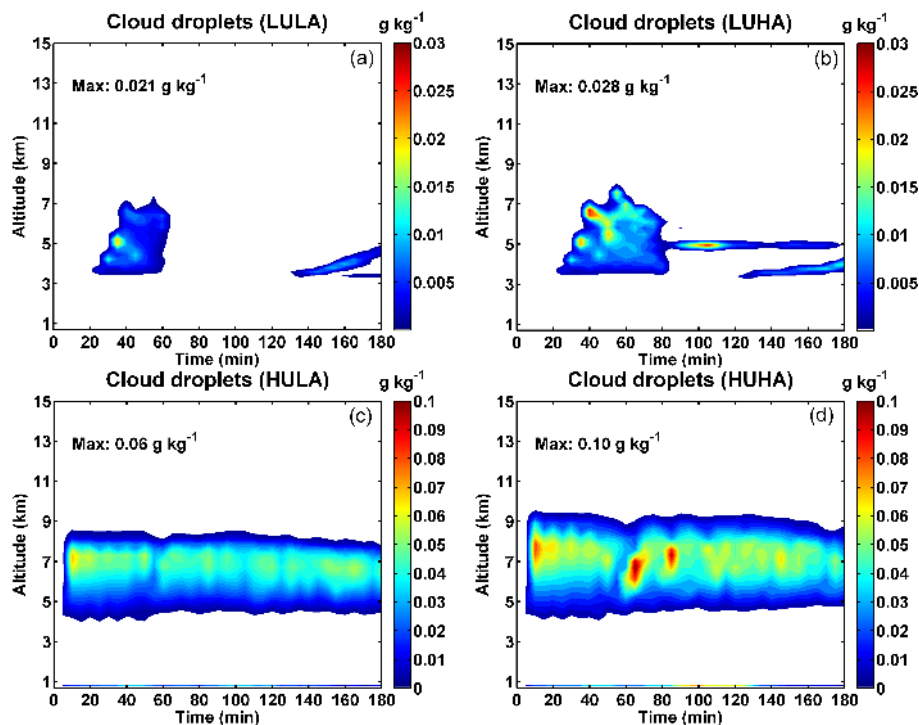


**Figure 6.** Time evolution of horizontally averaged cloud water content ( $\text{g kg}^{-1}$ ) as a function of altitude for four extreme cases, which are referred to as (1) LULA: low updrafts ( $2000 \text{ W m}^{-2}$ ) and low aerosols ( $200 \text{ cm}^{-3}$ ); (2) LUHA: low updrafts ( $2000 \text{ W m}^{-2}$ ) and high aerosols ( $100\,000 \text{ cm}^{-3}$ ); (3) HULA: high updrafts ( $300\,000 \text{ W m}^{-2}$ ) and low aerosols ( $200 \text{ cm}^{-3}$ ); and (4) HUHA: high updrafts ( $300\,000 \text{ W m}^{-2}$ ) and high aerosols ( $100\,000 \text{ cm}^{-3}$ ). Maximum values for each episode are also shown.

usually short (40–60 min). Under strong fire forcing conditions (HU), the cloud droplets form earlier (around 5 min), and most cloud droplets are located at a height of 5–9 km. Moreover, the cloud droplets reach steady state because of the cycling of cloud formation.

To investigate the sensitivity of an individual hydrometeor to changes in  $N_{\text{CN}}$  and FF, we adopted the definition of relative sensitivity  $\text{RS}_Y(X)$  (of one variable  $Y$  against the variable  $X$ ) as

$$\text{RS}_Y(X) = \frac{\partial Y/Y}{\partial X/X} = \frac{\partial \ln Y}{\partial \ln X}. \quad (1)$$

In this study,  $X$  is the factor affecting cloud formation, i.e.,  $N_{\text{CN}}$  and FF, and  $Y$  is the mass or number concentration of each hydrometeor type (cloud droplets, raindrops, and frozen particles). By using a natural logarithmic calculation of the variables (i.e.,  $X$ ,  $Y$ ), the percentage change in an individual parameter relative to its magnitude could be reflected better. This logarithmic sensitivity evaluation has been applied commonly in the assessment of aerosol–cloud interactions (Feingold, 2003; McFiggans et al., 2006; Kay and Wood, 2008; Reutter et al., 2009; Sorooshian et al., 2009; Karydis et al., 2012).

Figure 7a shows the dependence of cloud water droplets ( $N_{\text{CD}}$ ) on  $N_{\text{CN}}$  and FF. The shape of the isolines is generally consistent with the regime designations reported by Reutter

et al. (2009). Following Reutter et al. (2009), a value of the  $\text{RS}(N_{\text{CN}})$  to  $\text{RS}(\text{FF})$  ratio of 4 or 0.25 was taken as the threshold value to distinguish different regimes (the same criteria were employed for rainwater and frozen water content). Red dashed lines in Fig. 7a indicate the borders between different regimes. This resulted in an aerosol-limited regime in the upper left sector of the panel ( $N_{\text{CD}}$  is sensitive mainly to  $N_{\text{CN}}$  and is insensitive to fire forcing), an updraft-limited regime in the lower right sector of the panel ( $N_{\text{CD}}$  displays a linear dependence on FF and a very weak dependence on  $N_{\text{CN}}$ ), and the transitional regime along the ridge of the isopleth (FF and  $N_{\text{CN}}$  play comparable roles in the change in  $N_{\text{CD}}$ ). The regimes of Reutter et al. (2009) are derived from simulations of the cloud parcel model of CCN activation at the cloud base. Our results demonstrate that the general regimes for CCN activation still prevail, even when considering full microphysics and the larger temporal and spatial scales of a single pyro-convective cloud system. Figure 7c and d display the sensitivity of  $N_{\text{CD}}$  to variations in  $N_{\text{CN}}$  and FF. Note that the low/high-aerosol and fire forcing conditions (LA, HA, LU, and HU) in these figures refer to a group of  $N_{\text{CN}}$ /FF conditions – LU: low updrafts ( $1000$ – $7000 \text{ W m}^{-2}$ ); HU: high updrafts ( $75\,000$ – $300\,000 \text{ W m}^{-2}$ ); LA: low aerosols ( $200$ – $1500 \text{ cm}^{-3}$ ); and HA: high aerosols ( $10\,000$ – $100\,000 \text{ cm}^{-3}$ ). High sensitivities were found for low conditions of  $N_{\text{CN}}$  and FF. While there are some deviations (which appear to be ran-

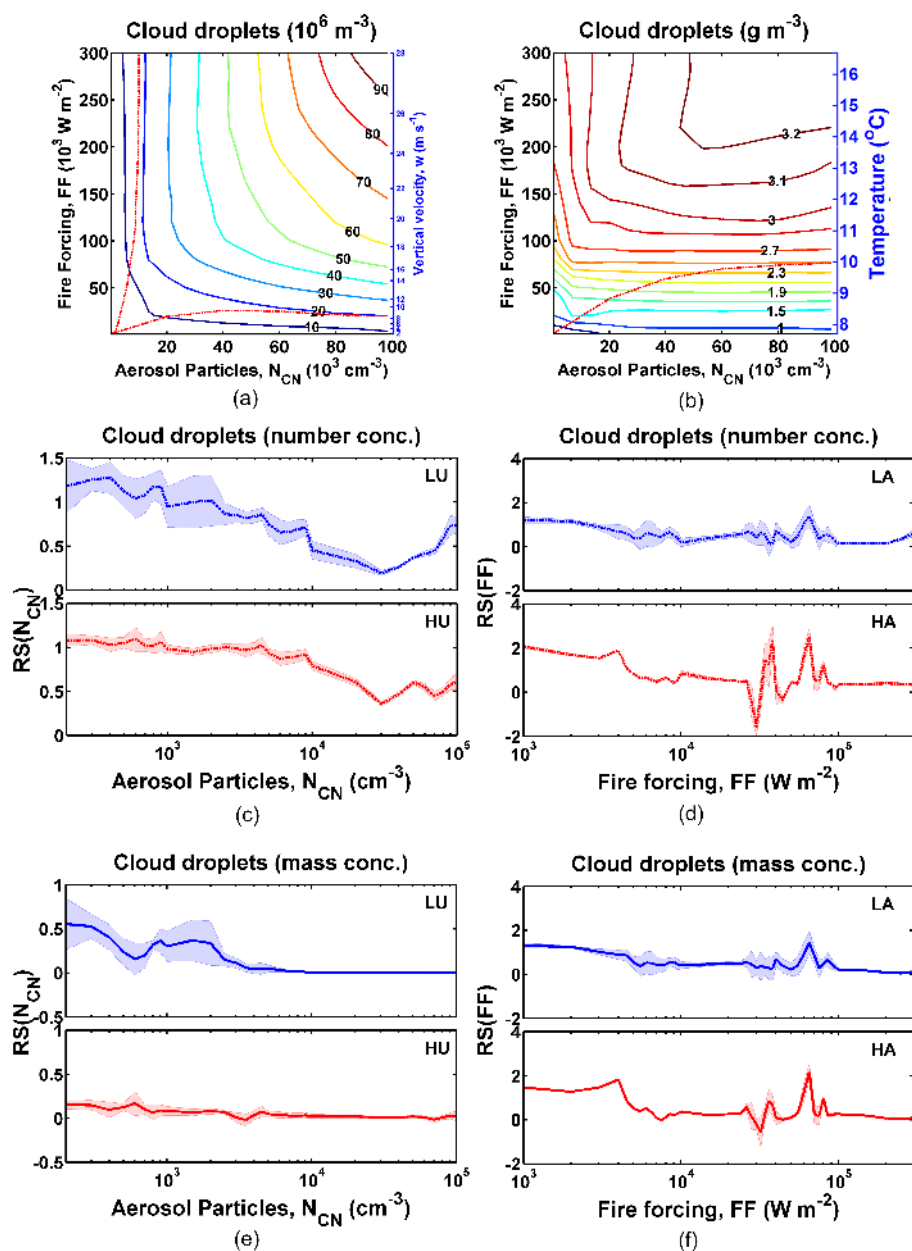


**Figure 7.** Number (a) and mass concentration (b) of cloud droplets calculated as a function of aerosol number concentration ( $N_{CN}$ ) and updraft velocity (represented by FF). Red dashed lines indicate the borders between different regimes defined by  $RS(N_{CN})/RS(FF) = 4$  or 0.25. Relative sensitivities with respect to  $N_{CN}$  (left) and FF (right) for number (panels c and d) and mass (panels e and f) concentration of cloud droplets under different conditions. The thick dashed or solid lines represent the mean values under a given condition, and the shaded areas represent the variability of estimation ( $\pm 0.5\sigma$ ). Abbreviations are as follows: LU, low updrafts (1000–7000  $\text{W m}^{-2}$ ); HU, high updrafts (75 000–300 000  $\text{W m}^{-2}$ ); LA, low aerosols (200–1500  $\text{cm}^{-3}$ ); and HA, high aerosols (10 000–100 000  $\text{cm}^{-3}$ ).

dom numerical noise), in general, as either  $N_{CN}$  or FF increases, the impact of further changes to either the variable on the cloud droplet number concentration becomes weaker (Fig. 7c and d). The reduced sensitivity of cloud droplets to aerosols can be explained by the buffering effect of the cloud microphysics, so that the response of the cloud system to aerosols is much smaller than would have been expected.

Compared with  $N_{CD}$ , the cloud mass concentration ( $M_{CD}$ ) is less sensitive to  $N_{CN}$ , and an aerosol-limited regime cannot be said to exist for  $M_{CD}$  (Fig. 7b and e). As a result, there are only two regimes indicated by the red dashed line in the contour plot (Fig. 7b): an updraft-limited regime in the lower right sector of the panel, and a transitional regime in the upper sector (an aerosol- and updraft-sensitive regime).

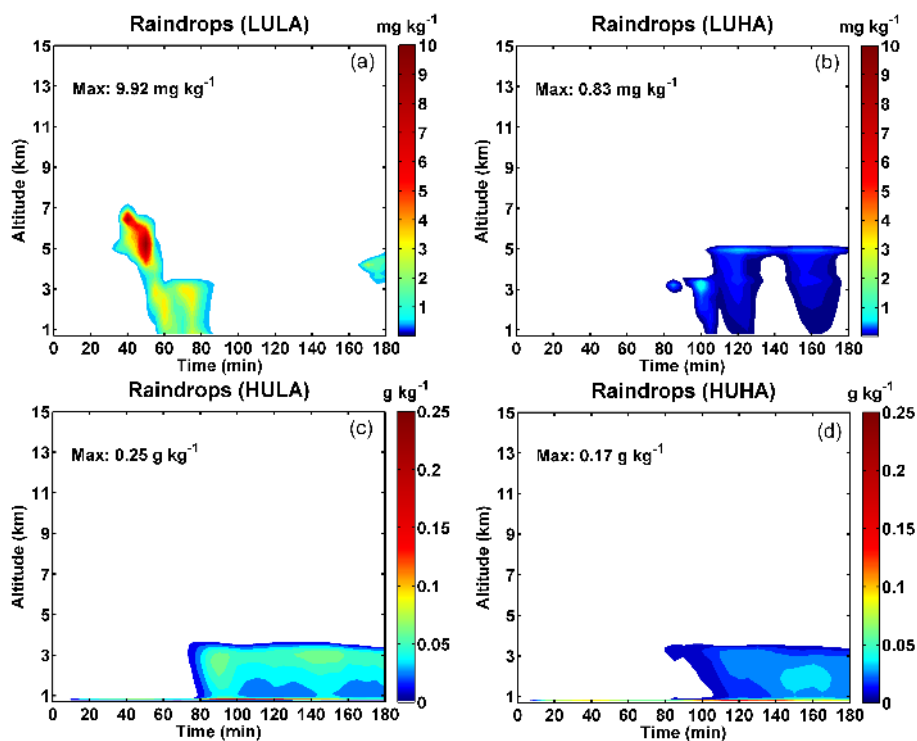


**Figure 8.** Same as Fig. 6 but for raindrops.

The  $RS(N_{CN})$  of  $N_{CD}$  is on average 10 times higher than that of  $M_{CD}$ , independent of the intensity of the FF. As  $N_{CN}$  increases,  $M_{CD}$  becomes insensitive to the change in  $N_{CN}$ . Averaged  $RS(FF)$  values over simulated FF ranges for  $N_{CD}$  (0.60) and  $M_{CD}$  (0.50) are commensurate (Fig. 7d and f, respectively), which implies that both the number and mass concentrations of cloud droplets are very sensitive to updrafts. These results are derived from simulations with persistent fire forcing over the modeling period. We have also examined the case in which the fire forcing was shut down after the first half hour of simulation (not shown). The same regimes were found in these simulations, with boundaries in good agreement with the findings presented in this work.

### 3.2.2 Raindrops

Figure 8 exhibits the temporal evolution of the horizontally integrated mass concentration of raindrops under four different conditions. Compared with cloud droplets (Fig. 6), the occurrence of raindrops is much later, especially when  $N_{CN}$  and fire forcing are at a high level. Only for the LULA case can numerous raindrops be found at a high altitude (5–7 km); for other cases, most of the raindrops are located below 5 km ( $\sim 0^\circ\text{C}$ ).

The response of the raindrop number concentration ( $N_{RD}$ ) to fire forcing and  $N_{CN}$  is more complex (Fig. 9a). The impact of FF on  $N_{RD}$  is non-monotonic. In general, enhanced FF leads to an increase in  $N_{RD}$  under weak updraft condi-

tions ( $< \sim 4000 \text{ W m}^{-2}$ ), while further increases in FF result in the reduction in  $N_{RD}$ . The aerosol influence varies in the course of  $N_{CN}$  change. Under low-aerosol conditions ( $< \sim 1500 \text{ cm}^{-3}$ ), increased  $N_{CN}$  can enhance the production of  $N_{RD}$ . Under high-aerosol conditions ( $> \sim 2000 \text{ cm}^{-3}$ ), the influence of  $N_{CN}$  on  $N_{RD}$  is very small.

As FF increases in magnitude, the amount of rain produced ( $M_{RD}$ ) increases (Fig. 9b), but the size of raindrops varies because of the complex behavior of the response of the raindrop number ( $N_{RD}$ ) to FF (Fig. 9a). The aerosol effect is non-monotonic:  $M_{RD}$  increases with aerosols in the lower range of  $N_{CN}$  values ( $< \sim 1000 \text{ cm}^{-3}$ ), but further increases in  $N_{CN}$  result in a decrease in  $M_{RD}$ . Combined with the relative sensitivities (Fig. 9e and f), the influence of FF is much more significant than that of  $N_{CN}$  in most cases. For example, the upper left corner (an aerosol-limited regime for  $N_{CD}$ ) becomes a transitional regime for  $M_{RD}$ , with  $RS(FF)$  of 0.1 and  $RS(N_{CN})$  of  $-0.06$  (Fig. 9). High sensitivities of  $M_{RD}$  to  $N_{CN}$  are found at low- $N_{CN}$  conditions, but the sensitivity decreases as  $N_{CN}$  increases (Fig. 9e). The  $N_{CN}$  plays the most negative role in  $M_{RD}$  under intermediate  $N_{CN}$  conditions ( $N_{CN}$  of several  $1000 \text{ cm}^{-3}$ ). In contrast to cloud droplet number concentration, an aerosol-limited regime for  $M_{RD}$  scarcely exists in our simulations (Fig. 9b). The response of the raindrops to aerosols is much weaker than the response of cloud droplets to aerosols. This finding is consistent with the idea of clouds acting as a buffered system formulated by Stevens and Feingold (2009). Detailed analy-



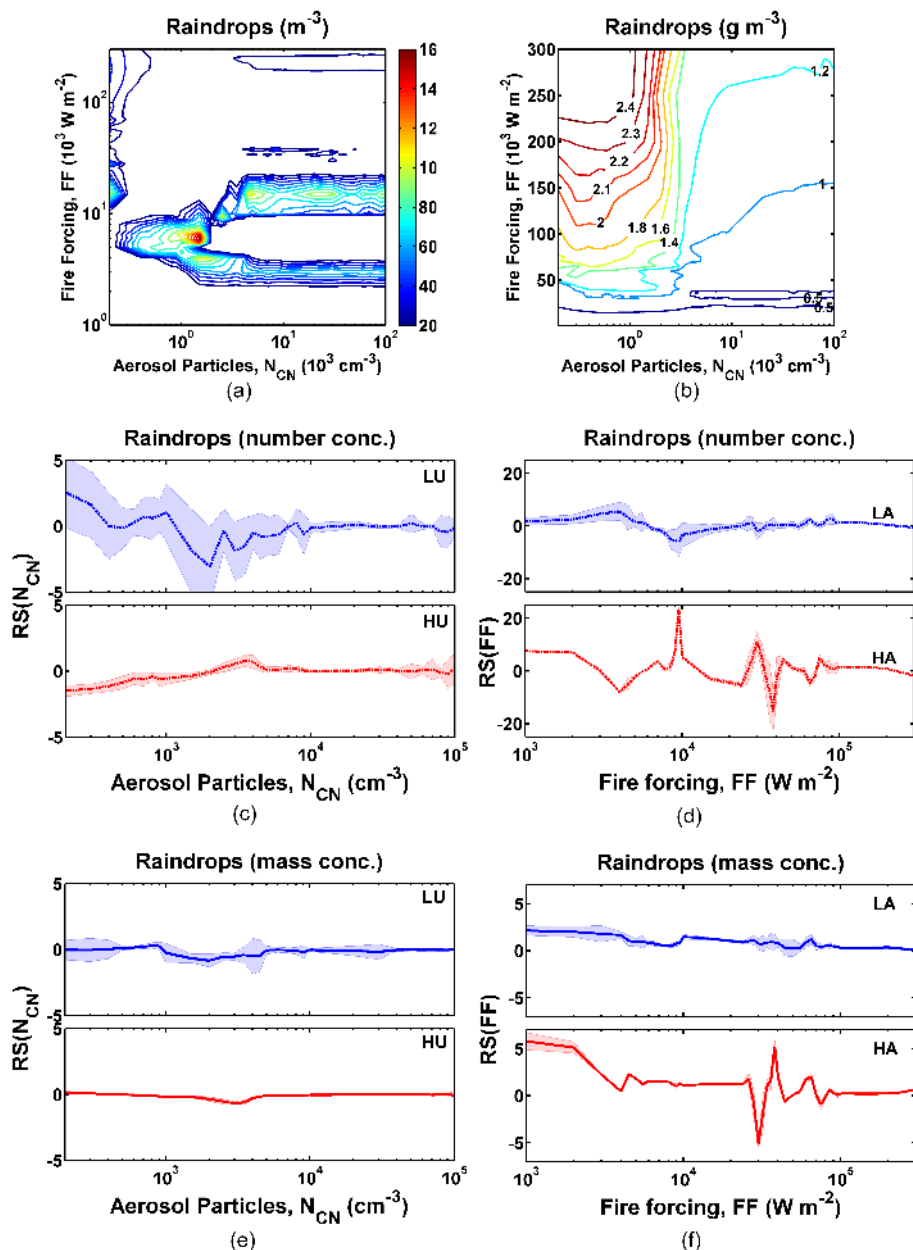


**Figure 9.** Same as Fig. 7 but for raindrops.

sis of the microphysical buffering processes will be presented in Sect. 3.3.2.

### 3.2.3 Frozen water contents

Within our microphysical scheme, frozen water contents are grouped into four main classes: ice crystals, snow, graupel, and hail (Seifert and Beheng, 2006). The time evolution of frozen water content in Fig. 10 suggests that the formation of frozen water content usually occurs at a high level (5–9 km for the LU case, and 7–13 km for the HU case), and the height of base layer and top layer decreases over time. Under LU

conditions, the appearance of frozen water content is around 35 min, and lasts for  $\sim 120$  min, with the peak concentration around 50–70 min. Under HU conditions, the frozen particles form around 10 min, and keep in a steady state.

Aerosols exert influence on the frozen water contents via the process of ice nucleation (in), but the processes that convert between the different hydrometeor classes and water vapor play a greater role in changing the concentrations of frozen particles, especially the processes of drop freezing to form ice (cfi) and the vapor condensational growth of ice and snow (vdi and vds, respectively). Figure 11 illustrates the percentage mass contributions of the individual frozen

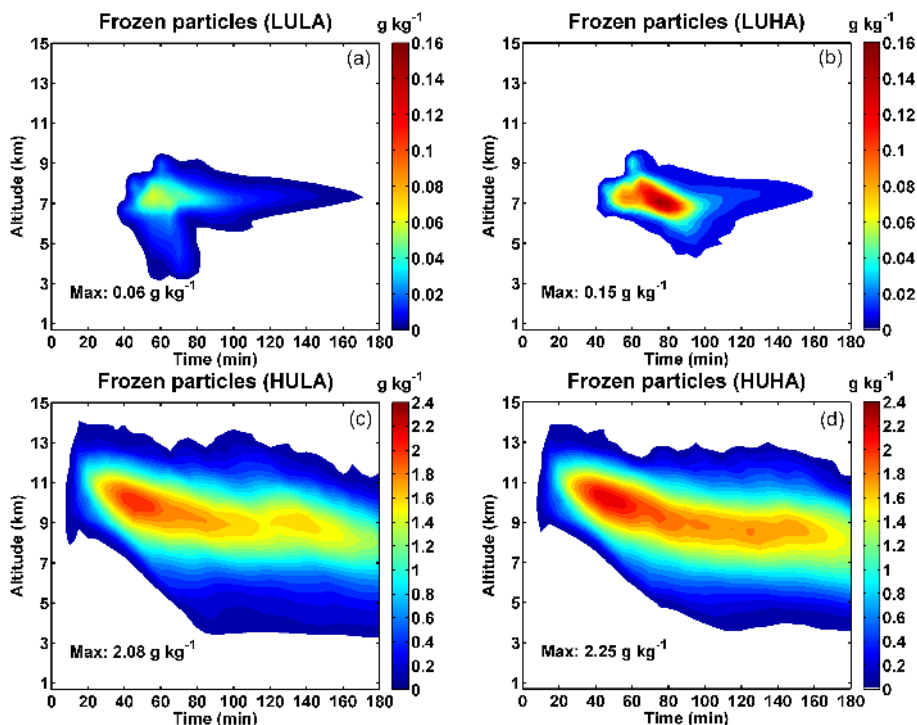


Figure 10. Same as Fig. 6 but for the frozen particles.

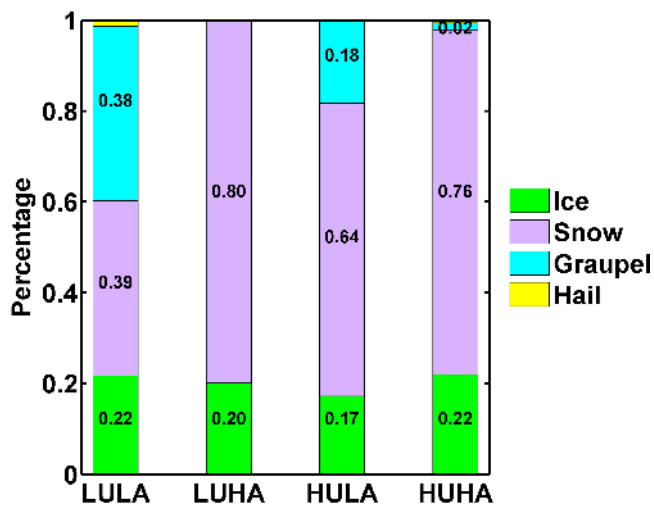
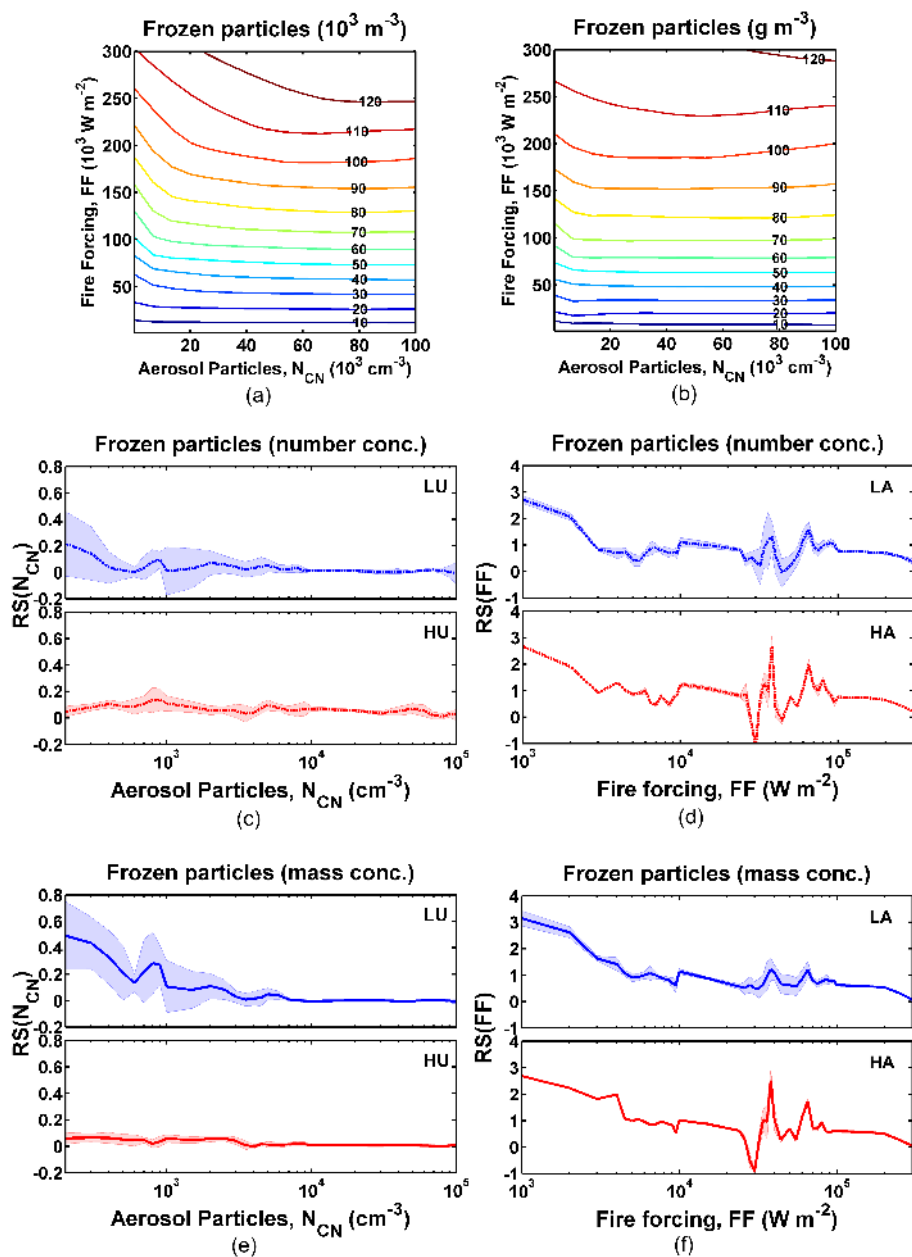


Figure 11. Contributions of individual frozen hydrometeor to total frozen water content under four extreme conditions, which are referred to as (1) LULA: low updrafts ( $2000 \text{ W m}^{-2}$ ) and low aerosols ( $200 \text{ cm}^{-3}$ ); (2) LUHA: low updrafts ( $2000 \text{ W m}^{-2}$ ) and high aerosols ( $100\,000 \text{ cm}^{-3}$ ); (3) HULA: high updrafts ( $300\,000 \text{ W m}^{-2}$ ) and low aerosols ( $200 \text{ cm}^{-3}$ ); and (4) HUHA: high updrafts ( $300\,000 \text{ W m}^{-2}$ ) and high aerosols ( $100\,000 \text{ cm}^{-3}$ ).

hydrometeor classes to the total frozen mass. The percentages of each hydrometeor are calculated based on average values over the entire simulation period. Generally, greater

concentrations of aerosols result in more snow and less graupel. This is in agreement with previous studies on convective clouds (Seifert et al., 2012; Lee and Feingold, 2013) and can be explained by the suppression of the warm rain processes under high-aerosol conditions. High  $N_{\text{CN}}$  delays the conversion of the cloud water to form raindrops, so that more cloud water content can ascend to altitudes with sub-zero temperatures and hence freeze into small frozen particles (Rosenfeld et al., 2008). Other research has suggested that elevated aerosols could increase the concentration of large frozen particles (graupel/hail) in the convective system (Khain et al., 2009; Wang et al., 2011), which was attributed to the competing effects of aerosols on graupel formation. Since graupel is mainly formed by the accretion of supercooled droplets by ice or snow, the smaller but more abundant supercooled drops under polluted conditions could be either favorable or unfavorable for graupel formation. The percentage of ice crystals does not change much, with ice crystals contributing approximately 20% on average to total frozen particle mass (Fig. 11). It is worth noting that stronger FF leads to increasing concentration of hail. But compared to other hydrometeors, its contribution is not important and the relative percentage is very low.

The dependence of total frozen particles on FF and  $N_{\text{CN}}$  is summarized in Fig. 12. With the enhancement in FF and  $N_{\text{CN}}$ , both the number and mass concentrations of the frozen water particles ( $N_{\text{FP}}$  and  $M_{\text{FP}}$ , respectively) increase. High  $\text{RS}(N_{\text{CN}})$  and  $\text{RS}(\text{FF})$  values were found under low- $N_{\text{CN}}$



**Figure 12.** Same as Fig. 7 but for total frozen particles.

and FF conditions (Fig. 12), respectively. As  $N_{\text{CN}}$  or FF increases, its impact becomes weaker, as indicated by a decreasing RS. According to the ratio of  $\text{RS}(\text{FF})/\text{RS}(N_{\text{CN}})$ , both  $N_{\text{FP}}$  and  $M_{\text{FP}}$  are within the updraft-limited regime. Again, smaller  $\text{RS}(N_{\text{CN}})$  values for  $M_{\text{FP}}$ , compared with  $N_{\text{CD}}$ , illustrate the weaker impact of  $N_{\text{CN}}$  on the production of frozen particles.

### 3.2.4 Precipitation rate

Surface precipitation rate is a key factor in climate and hydrological processes. Many field measurements, remote sensing

studies, and modeling simulations have attempted to evaluate the magnitude of aerosol-induced effects on the surface rainfall rate (Rosenfeld, 1999, 2000; Tao et al., 2007, 2012; Li et al., 2008; Sorooshian et al., 2009). Figure 13a shows the response of surface precipitation rate (averaged over each 3 h simulation) to FF and  $N_{\text{CN}}$ . The response of surface precipitation to these forcings is similar to that of raindrops (Fig. 9b). FF plays a positive role in the precipitation, and  $\text{RS}(\text{FF})$  shows a decreasing trend as FF increases (Fig. 13c).

The effect of  $N_{\text{CN}}$  is more complex. Both positive and negative  $\text{RS}(N_{\text{CN}})$  were found in our study. There are gener-

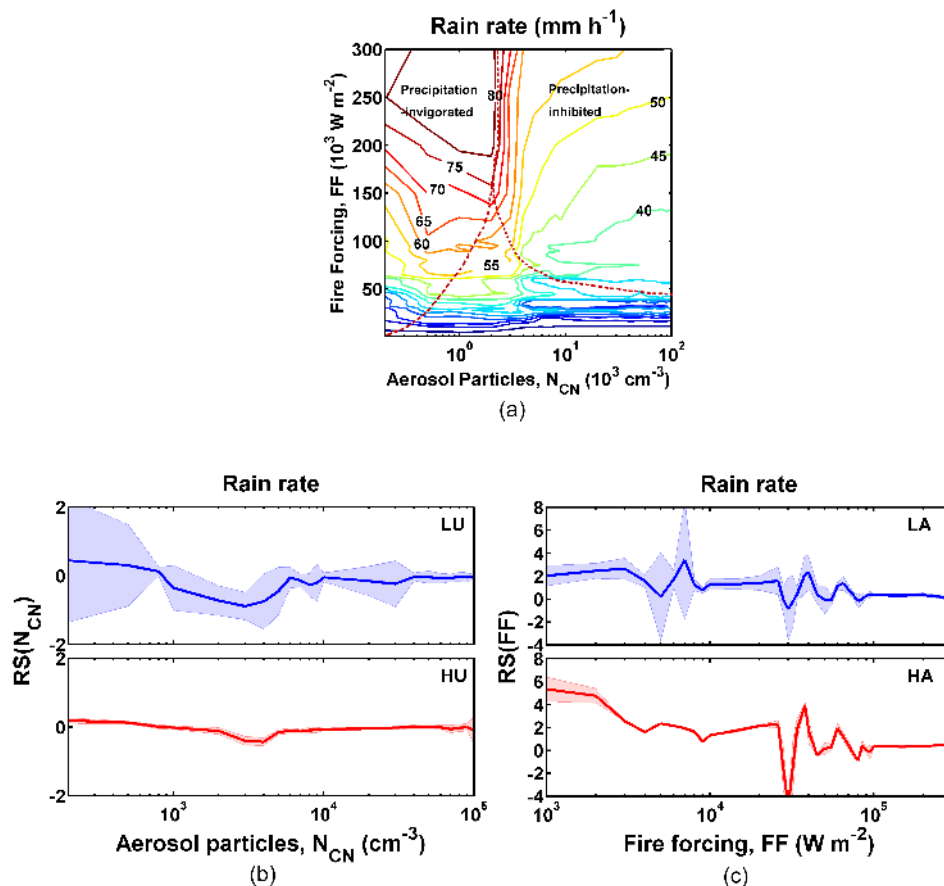


Figure 13. Same as Fig. 7 but for surface rain rate.

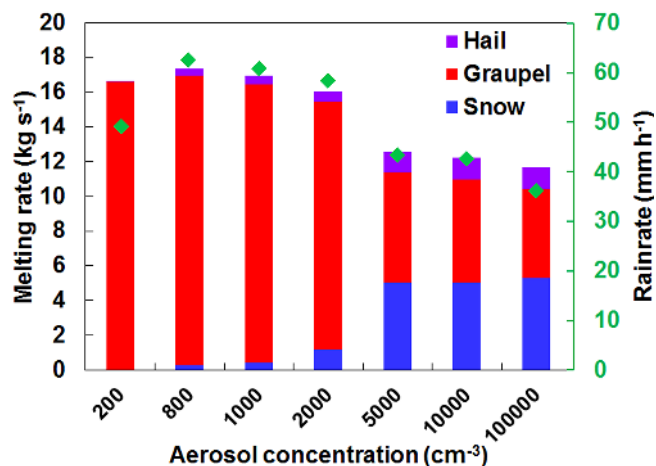
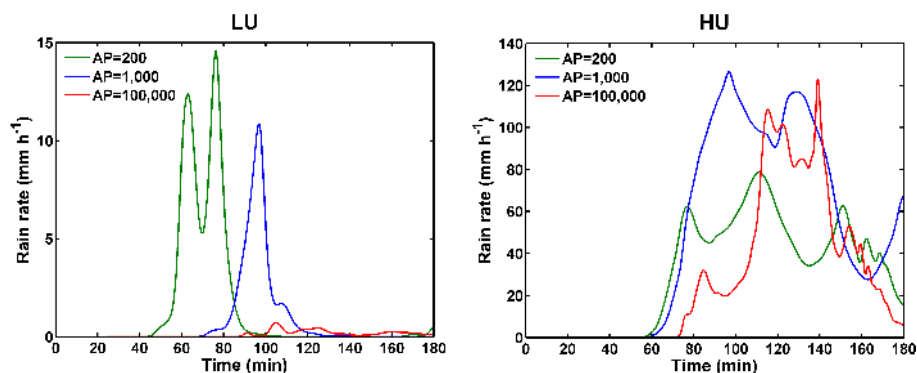


Figure 14. The correlation of rain rate and the melting rate of the frozen particles. The green diamond points are the averaged rain rate under different aerosol concentrations ( $FF = 10^5 \text{ W m}^{-2}$ ). The columns represent the integrated melting rate from individual frozen particles.

ally two different regimes: a precipitation-invigorated regime and a precipitation-inhibited regime. In the precipitation-invigorated regime ( $N_{CN} \sim 1000 \text{ cm}^{-3}$ ), an increase in  $N_{CN}$  leads to an increase in the precipitation rate, and a reduction in  $RS(N_{CN})$  (Fig. 13b). In the precipitation-inhibited regime ( $N_{CN} > \sim 1000 \text{ cm}^{-3}$ ), aerosols start to reduce the precipitation, which is reflected in a negative  $RS(N_{CN})$ . Within the precipitation-inhibited regime, there is also an extreme  $RS(N_{CN})$  at a value of  $N_{CN}$  of a few thousand particles per cubic centimeter (Fig. 13b). The threshold to distinguish these two regimes is derived from the current simulated pyro-convective clouds. The cumulus cloud investigation in Li et al. (2008) also suggested this non-monotonic trend, with the threshold aerosol value around  $3000 \text{ cm}^{-3}$ . The existence of threshold  $N_{CN}$  in both studies implies that similar cloud types may have a similar regime dependence, of which the exact shape may differ due to difference in the meteorological conditions, aerosol properties, etc.

Based on the ensemble studies, we found that individual case studies result in large uncertainties in evaluating the response of precipitation to perturbations, e.g.,  $N_{CN}$ . Different selections of the parameter space may result in different or even opposite conclusions. Therefore, our ensemble study



**Figure 15.** Time evolution of surface rain rates for the three aerosol episodes ( $N_{\text{CN}} = 200, 1000, \text{ and } 100\,000\text{ cm}^{-3}$ , respectively) under LU (low updrafts,  $\text{FF} = 2000\text{ W m}^{-2}$ ) and HU (high updrafts,  $\text{FF} = 50\,000\text{ W m}^{-2}$ ) conditions.

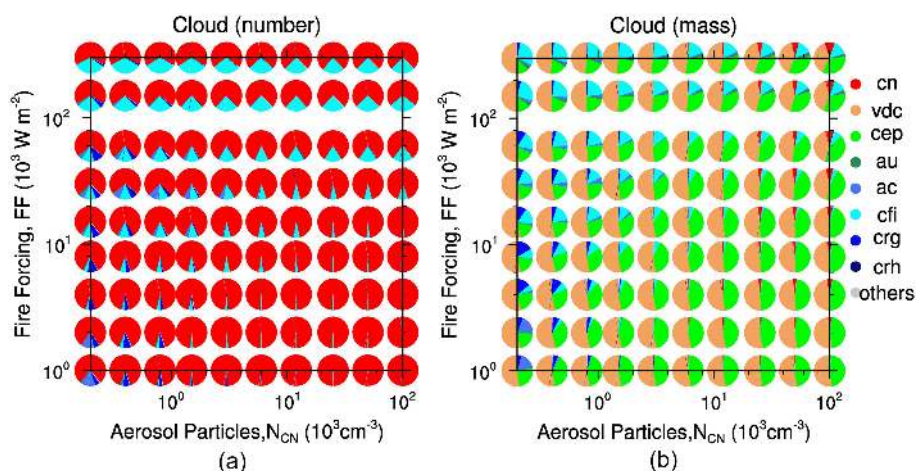


**Figure 16.** The pie charts summarize the relative percentage of the microphysical processes involving cloud droplets as a function of  $N_{\text{CN}}$  and fire forcing (**a** number concentration, **b** mass concentration). Colors within each pie chart reflect the contribution of processes under the specific condition. Warm colors denote the sources, while cold colors denote the sinks. Abbreviations are as follows: cn, cloud nucleation; vdc, condensational growth of cloud droplets; cep, evaporation of cloud droplets; au, autoconversion; ac, accretion; cfi, freezing of cloud droplets to form ice crystals, including homogeneous and heterogeneous nucleation; and crg/h, riming of cloud droplets to form graupel/hail.

over a wide range of parameter space sheds some light on these debates.

Within our simulations, melting of frozen particles is the biggest contributor to precipitation, and the rain rate is well correlated with the melting rate (Fig. 14). For  $N_{\text{CN}} > 1000\text{ cm}^{-3}$ , increasing  $N_{\text{CN}}$  results in more small frozen particles (i.e., snow) with low fall velocities. These small frozen particles cannot fall into the warm areas and melt efficiently, resulting in a reduced melting rate. For  $N_{\text{CN}} < 1000\text{ cm}^{-3}$ , the ratio between large and small frozen particles is not sensitive to  $N_{\text{CN}}$  anymore and the vertical distribution of frozen particles becomes important. Increasing  $N_{\text{CN}}$  leads to earlier formation of frozen particles at low altitude, which evaporate less and result in more rainfall.

In the literature, both positive (Tao et al., 2007) and negative (Altartatz et al., 2008) relationship between aerosols and rain rate have been reported in previous case studies. Our

simulations suggest that this apparently contradictory phenomenon might be the expression of the same physical processes under different aerosol and dynamic conditions.

Regarding the temporal evolution, low  $N_{\text{CN}}$  results in earlier rainfall (Fig. 15), which is consistent with current understanding, observations (e.g., Rosenfeld, 1999, 2000), and modeling evidence (e.g., the convective cumulus cloud study by Li et al., 2008). Note that the general relationship between precipitation and aerosols described in this study is based on simulations over a period of 3 h. Simulations for a longer period should be carried out in future studies to investigate the influence of aerosols on precipitation over longer timescales as in Fan et al. (2013) and Wang et al. (2014).

### 3.3 Process analysis

In our simulations, the evolution of hydrometeor concentrations is determined by multiple microphysical processes. It

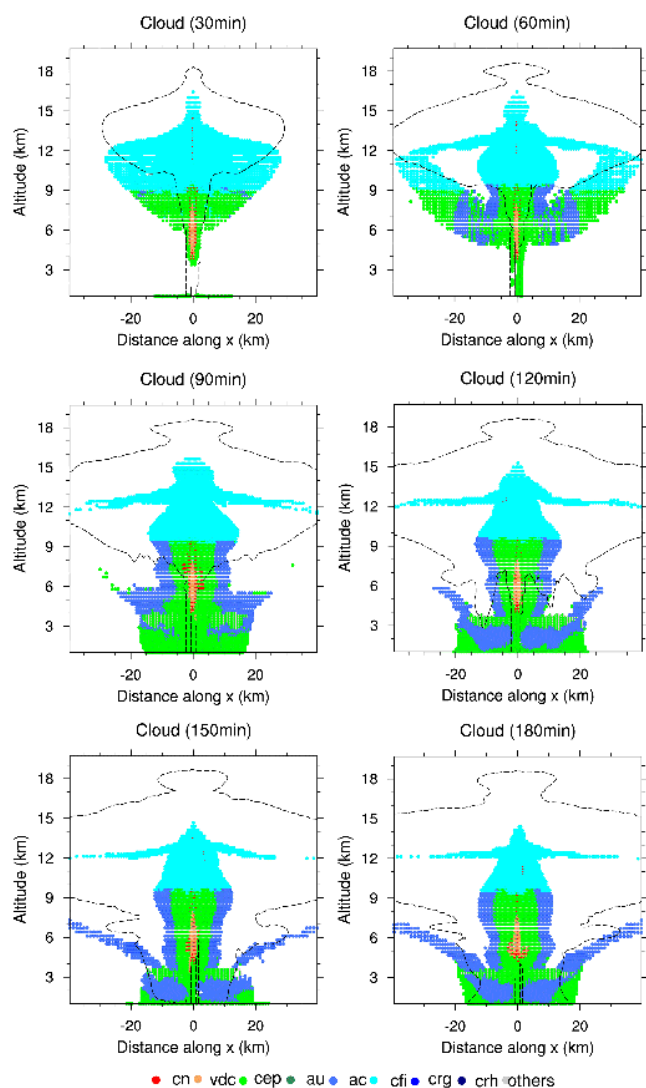


**Figure 17.** The pie charts summarize the vertical cross sections of the rate of change of main microphysical processes contributing to cloud water content. Each pie chart shows the averaged contribution over the past 30 min. Colors within each pie chart reflect the percentage of processes in each grid. The black dashed line is the  $0.1 \mu\text{g kg}^{-1}$  isoline of the interstitial aerosol, indicating the shape of smoke plume. The meaning of the abbreviations is the same as in Fig. 16. Warm colors denote the sources, while cold colors denote the sinks.

is often difficult to tell exactly how aerosol particles affect clouds and precipitation. Here we introduce a process analysis method to help understand the aerosol effects.

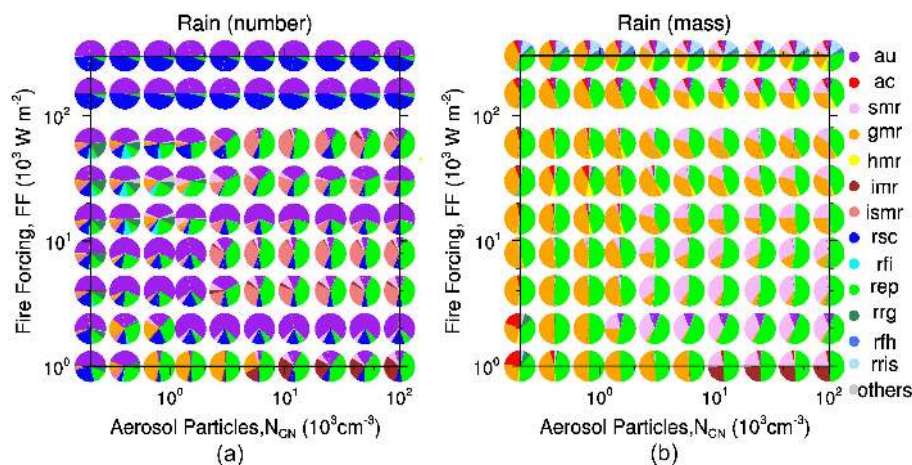
### 3.3.1 Clouds

Figure 16 summarizes the contribution of the microphysical processes that act as the main sources (warm colors) and sinks (cold colors) for cloud droplets under different aerosol and fire forcing conditions. For  $N_{\text{CD}}$ , the dominant

source term is the cloud nucleation (CCN activation) process, in which aerosols are activated under supersaturated water vapor and form cloud droplets. As cloud nucleation happens mostly at the cloud base and thus is not strongly affected by cloud dynamical feedbacks, the response of  $N_{\text{CD}}$  shows similar regimes to cloud parcel models (Reutter et al., 2009). To help explain the regime designation, we divide  $N_{\text{CD}}$  into two factors: an ambient aerosol number concentration ( $N_{\text{CN}}$ ) and an activated fraction ( $N_{\text{CD}}/N_{\text{CN}}$ ). Given the aerosol size distributions, the  $N_{\text{CD}}/N_{\text{CN}}$  ratio is determined approximately by the critical activation diameter ( $D_c$ ) above which the aerosols can be activated into cloud droplets. The  $D_c$  is a function of ambient supersaturation. Stronger updrafts result in higher supersaturation, smaller  $D_c$  and hence larger  $N_{\text{CD}}/N_{\text{CN}}$  ratios. Under high-updraft conditions ( $> 15 \text{ m s}^{-1}$ ),  $N_{\text{CD}}/N_{\text{CN}}$  is already close to unity (Reutter et al., 2009). A further increase in the updraft velocity will still change the supersaturation and  $D_c$ , but it will not significantly influence the  $N_{\text{CD}}/N_{\text{CN}}$  ratios and  $N_{\text{CD}}$ . In this case,  $N_{\text{CD}}$  is approximately proportional to  $N_{\text{CN}}$ .

Under weak updrafts, the  $N_{\text{CD}}/N_{\text{CN}}$  ratio is sensitive to ambient supersaturations. In this case, a larger supersaturation induced by stronger updrafts can effectively change the  $N_{\text{CD}}/N_{\text{CN}}$  ratio, and thus  $N_{\text{CD}}$  is sensitive to the updraft velocity. On the other hand, the stronger dependence of  $N_{\text{CD}}/N_{\text{CN}}$  on the supersaturation also changes the role of aerosols. As more aerosols reduce supersaturation, increasing  $N_{\text{CN}}$  tends to reduce the activated fraction,  $N_{\text{CD}}/N_{\text{CN}}$ . Taking  $N_{\text{CN}} = 60\,000 \text{ cm}^{-3}$  ( $\text{FF} = 2000 \text{ W m}^{-2}$ ), for example, a 10% increase in  $N_{\text{CN}}$  causes a 4% decrease in  $N_{\text{CD}}/N_{\text{CN}}$ , whereas a 10% decrease in  $N_{\text{CN}}$  leads to an 8% increase in  $N_{\text{CD}}/N_{\text{CN}}$ . The impact of changing  $N_{\text{CN}}$  on the  $N_{\text{CD}}/N_{\text{CN}}$  ratio counteracts partly or mostly the positive effect of  $N_{\text{CN}}$  on cloud droplet formation.

The changes in  $M_{\text{CD}}$  are influenced mainly by (sources) (1) the condensation of water vapor on the present cloud droplets (vdc) and (2) the cloud nucleation process (cn) and by (sinks) (3) cloud droplet evaporation (cep), (4) the accretion of cloud droplets (ac), and (5) the freezing of cloud droplets to form cloud ice (cfi), the latter of which includes heterogeneous (Seifert and Beheng, 2006) and homogeneous freezing processes (Jeffery and Austin, 1997; Cotton and Field, 2002). Concerning their relative contributions, the net change in condensational growth of droplets (vdc) and cloud droplet evaporation (cep) dominates the change in  $M_{\text{CD}}$ . As  $N_{\text{CN}}$  increases, the condensation rate (vdc) does not change much, while the evaporation rate (cep) is raised greatly owing to increased surface-to-volume ratio of smaller cloud droplets. Condensation increases  $M_{\text{CD}}$  and evaporation reduces  $M_{\text{CD}}$ . In our study, the net effects are negative. A similar result was reported by Khain et al. (2005) for deep convective clouds. They found that high CCN concentrations led to both greater heating and cooling, and that the net convective heating became smaller as CCN increased. However, the cloud nucleation rate is enhanced and the loss of cloud wa-



**Figure 18.** Same as Fig. 16 but for raindrops. Abbreviations are as follows: au, autoconversion; ac, accretion; *i/s/g/hmr*, melting of ice/snow/graupel/hail to form raindrops; rsc, self-collection of raindrops; ismr, melting of ice and snow to form raindrops; rfi/h, freezing of raindrops to form ice crystals/hail; rep, raindrop evaporation; rrg, riming of raindrops to form graupel; and rris, riming of raindrops to form ice and snow.

ter due to other sinks (ac for weak FF conditions, and cfi for strong FF conditions) decreases at the same time. This leads to an increasing trend in the total cloud water content with the increase in  $N_{CN}$ .

Concerning the absolute contribution, increasing FF enhances the change rate of the conversion of water vapor to the condensed phase ( $R_{vdc}$  and  $R_{cn}$ ), whose effect is straightforward. The processes of autoconversion (au) and accretion (ac) are the major sinks at weak updrafts. As FF increases, the conversion of cloud droplets to frozen particles, especially to ice (the cfi process), becomes increasingly important.

The contribution of the microphysical processes in each modeling grid can be observed from the pie charts in Fig. 17 (taking HUHA ( $w = 27 \text{ m s}^{-1}$ ;  $N_{CN} = 100\,000 \text{ cm}^{-3}$ ) for example, which is representative of the pyro-convective clouds). Each plot shows the vertical cross sections of the averaged change rate of main processes contributing to cloud water content over 30 simulation minutes. Colors within each pie chart reflect the percentage of contributions in each grid. CCN activation usually starts at cloud base, followed by vdc in the center of the cloud. Towards both sides, cloud droplets convert to water vapor via evaporation. It is worth noting that the pie charts only represent the relative importance of each process at individual simulation grid, not the absolute amount. Though there are fewer vdc-dominated grids than cep-dominated grids, the total cloud formation rate from vdc is still similar to or higher than the cep processes. At cloud top with sub-freezing temperature, cloud droplets are frozen to ice crystals via homogeneous and heterogeneous nucleation. At the beginning stage of the cloud (30 min), the cloud droplets concentrate at the center of the modeling domain. As the cloud evolves, it starts to expand, and at the same time the

margin area dissipates due to the sink processes (i.e., cep, cfi, and ac).

We are aware that the exact process rates may vary depending on the microphysical schemes used in the simulation (Muhlbauer et al., 2010). Therefore, we stress that the process analysis here is based on the Seifert microphysical scheme (Seifert and Beheng, 2006). In the future, further observations from laboratory and field measurements are needed to improve the understanding of aerosol–cloud interactions and to better constrain microphysical parameterizations.

### 3.3.2 Rain

Dynamic conditions strongly influence the pathways of rain formation and dissipation. For weak updraft cases, the warm rain processes, i.e., autoconversion (au) and accretion (ac), play a big role. Together with melting of snow (smr) or graupel (gmr), they are the main sources for raindrops (Fig. 18). Under this condition, raindrops may appear at altitudes as high as 5–7 km (e.g., Fig. 8a). For high updraft cases, strong updrafts deliver cloud droplets to higher freezing altitudes (Fig. 6). The cloud droplets then turn directly into frozen particles (cloud→ice crystals), without formation of raindrops as an intermediate stage (cloud→rain→larger frozen particles). Most raindrops are formed from melted frozen droplets, and consequently they appear below  $\sim 4$  km (Fig. 8c, d). The weaker cloud→rain conversion with higher updrafts also influences the conversion of rain to frozen particles and is the reason why the rrg process (riming of raindrops to form graupel) becomes relatively less important as FF increases under low-aerosol conditions.

The aerosols also modify the pathways of rain formation. Taking weak updraft cases, for example, the accretion pro-

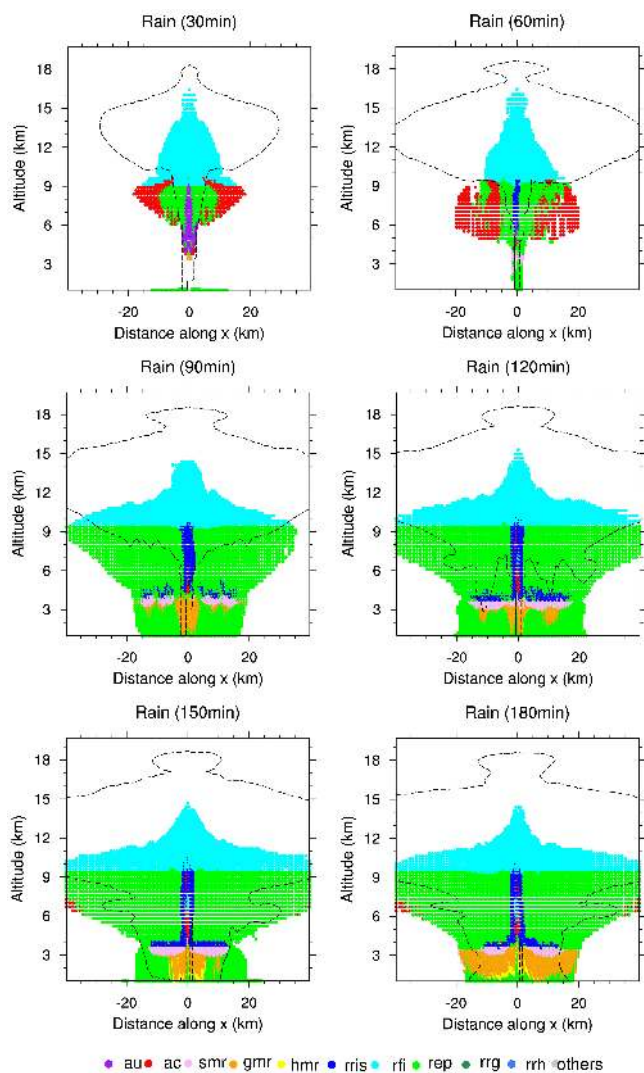


**Figure 19.** Same as Fig. 17 but for raindrops.

cess (ac) dominates the cloud  $\rightarrow$  rain conversion under low aerosol concentrations but is replaced by autoconversion (au) under high aerosol concentrations (Fig. 18b). The reason for this is that au is the process that initializes rain formation. Once rain embryos are produced, accretion of cloud droplets by raindrops is triggered and becomes the dominant process of rainwater production, as observed for shallow clouds (Stevens and Seifert, 2008) and stratiform clouds (Wood, 2005). High aerosol loading delays the occurrence of au, inhibiting the initialization of rain and the following accretion processes at the early stage (0–100 min). Melted frozen particles are also a major source of raindrops. Under low- $N_{CN}$  conditions, most of them form from melted graupel particles, whereas under high- $N_{CN}$  conditions, melting of snowflakes becomes more important. This is consistent with the aerosol impact on the relative abundance of frozen particles shown in Fig. 11. A higher aerosol concentration leads

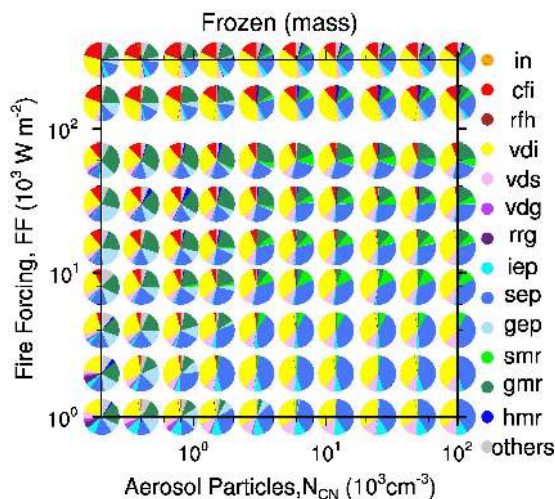


**Figure 20.** Same as Fig. 16 but for the total frozen water content. Abbreviations are as follows: in, ice nucleation; cfi, freezing of cloud droplets to form ice crystals, including homogeneous and heterogeneous nucleation; rfh, freezing of raindrops to form hail; vdi/s/g, condensational growth of ice crystals/snow/graupel by water vapor; rrg, riming of raindrops to form graupel; i/s/gep, evaporation of ice/snow/graupel; s/g/hmr, melting of snow/graupel/hail to form raindrops.

to a higher fraction of smaller frozen particles (ice crystals and snowflakes). The main difference between low and high updrafts is that cloud conversion is the main source in the former case, whereas melted graupel/snow particles become the main contributors in the latter case.

Figure 19 illustrates the temporal evolution of the contribution of each process at individual simulation grid (HUHA case). As mentioned before, the warm rain process is quite unimportant under strong FF conditions (Fig. 18b). However, it is observed that the warm rain process is the leading source of raindrops at the beginning stage (60 min). The raindrops formed from au and ac are relatively small, and can easily evaporate. The melting of frozen particles to form raindrops becomes more significant after  $\sim 90$  min, which dominates the production of raindrops. As shown in Fig. 19, although the processes still continue at 180 simulation minutes, the microphysics have already fully developed during this simulation period. Thus our three simulation hours could cover the characteristics of the formation and evolution of the pyro-convective clouds. What is more, attention should be paid to the fact that long-term simulation may conceal some detailed information, leading to the bias in prediction of hydrometeor.

The PA clearly demonstrates that aerosols could significantly alter the microphysical pathways and their intensities. Although the variation in individual microphysical process is remarkable, the net result of all processes is not obvious and even insusceptible to aerosol perturbations. This is especially obvious when we consider the aerosol effect on rain water:



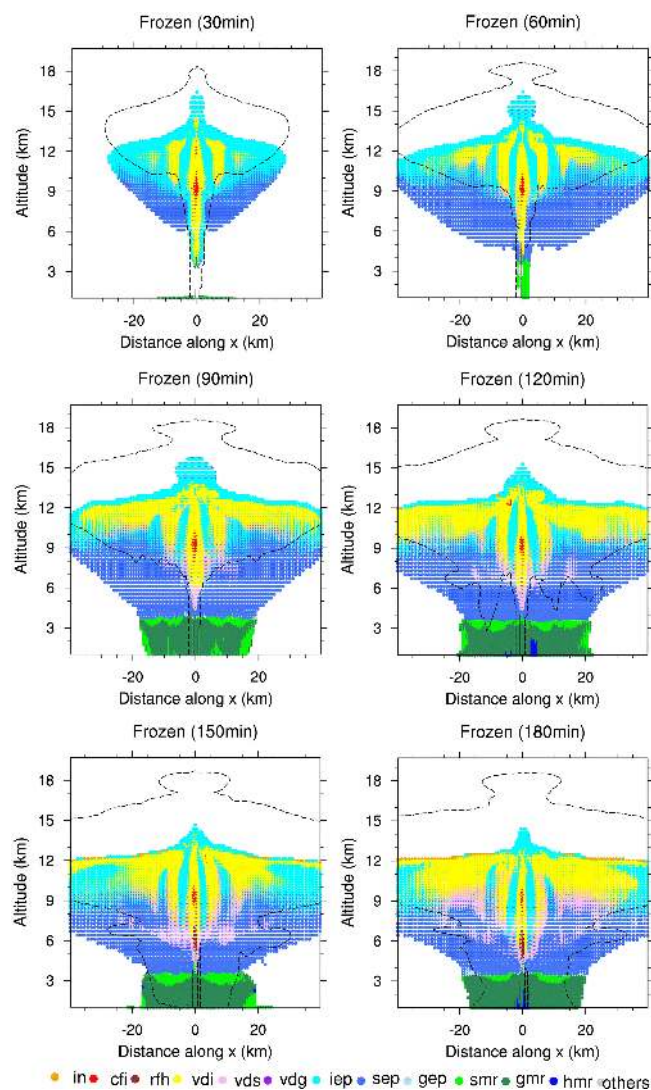


Figure 21. Same as Fig. 17 but for frozen particles.

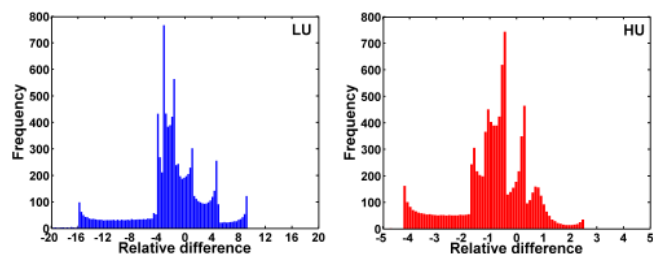


Figure 22. Histograms of the relative difference between  $\frac{\Delta Y}{\Delta N_{CN}}$  and  $\frac{dY}{dN_{CN}}$  under LU and HU conditions, where  $Y$  here denotes precipitation rate.  $\frac{\Delta Y}{\Delta N_{CN}} = \frac{Y(2N_{CN}) - Y(N_{CN})}{2N_{CN} - N_{CN}}$ , and  $\frac{dY}{dN_{CN}}$  is the derivative of the precipitation rate along the variable  $N_{CN}$ .

it is observed that, as aerosol is enhanced by a factor of 500, the intensities of the source processes only decrease by a factor of 10; however, there is only a 2-fold change in the net

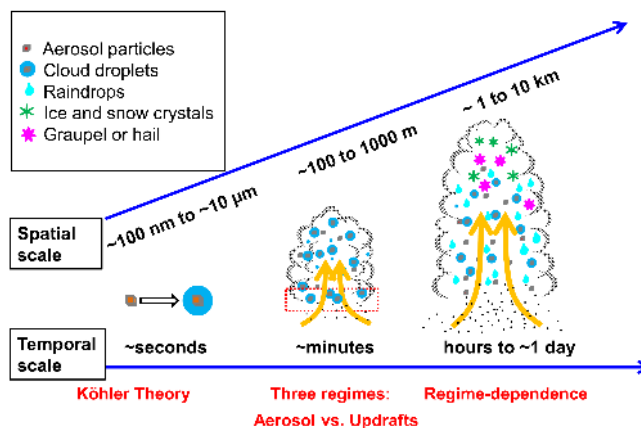


Figure 23. Overview of the research approaches on multi-scale cloud initialization and development. The aerosol–cloud interaction at the microphysical scale, i.e., cloud condensation nuclei (CCN) activation, has been well characterized by the Köhler theory (Köhler, 1936) and by a series of extended equations (Shulman et al., 1996; Kulmala et al., 1997; Laaksonen et al., 1998). When we upscale the activation of a single aerosol particle to aerosol populations at the cloud base, the impact of aerosols on the number of activated CCN still appears simple and can be well described (i.e., the three generic regimes of CCN activation). When considering full microphysics and the larger temporal and spatial scales of a single pyro-convective cloud, the performance of ensemble simulations shows the regime dependence of aerosol effects on the pyro-convective cloud formation and evolution.

rain water content. This implies that the cloud microphysics itself is a self-regulatory system, which can produce equilibrium and buffers the effect of aerosol disturbance (negative feedback).

The sensitivity of raindrops to aerosols mainly depends on autoconversion parameterization, the melting processes, etc. All those parameterizations have very large uncertainties, especially with bulk microphysical parameterizations. For example, most of the autoconversion schemes were developed or evaluated for stratocumulus clouds, which may not be appropriate for convective clouds. Based on the simulations during the convective phase of squall-line development, van Lier-Walqui et al. (2012) presented the uncertainty in the microphysical parameterization by the posterior probability density functions (PDFs) of parameters, observations, and microphysical processes. With the purpose to improve the representation of microphysics, it is of significance to quantify the parameterization uncertainty by using observation data to constrain parameterization.

### 3.3.3 Frozen water content

In this section, we only focus on the interactions between liquid water phase and solid water phase. As the self-collection and internal conversion between different frozen hydrometeors could also cause the change in number concentration

of total frozen particles, the process analysis for its number concentration is not discussed. As shown in Fig. 20, the effect of FF is straightforward, boosting vapor deposition (vdi) and cloud droplet freezing on ice (cfi). The vdi is always the most important pathway for the formation of frozen particles in our simulations, whereas cfi shows comparable contribution in the HULA case. Over a wide range of  $N_{CN}$  and updraft velocities, our results have extended and generalized the results of Yin et al. (2005), in which vdi and cfi were suggested as the dominant processes controlling the formation of ice crystals in individual mixed-phase convective clouds. Although snow is the dominant constituent of frozen particle mass (Fig. 11), the condensation of vapor on ice (vdi) rather than on snow is the major pathway for frozen particles. The increase of snow mass is mostly caused by collecting of ice (ics) and ice self-collection (coagulation of ice particles, iscs), which are internal conversions not counted as either a source or a sink of frozen water content. The ice crystals used for conversion to snow derive mostly from the vdi process. Increasing FF enhances the upward transport of water vapor and liquid water to higher altitudes, where frozen particles can be formed effectively through vdi and cfi. On the other hand, stronger FF reduces the residence time of cloud droplets in the warm environment (to form raindrops), which could explain the attenuation of rrg (riming of raindrops to form graupel) as fire forcing increases under low-aerosol conditions.

Positive relationship between aerosols and the frozen water content have been demonstrated in Sect. 3.2.3. As shown in Fig. 20, the increase in frozen water content is achieved through the enhancement of the vdi process. The condensational growth rate  $R_{vdi}$  is a function of the number concentration ( $N_{ice}$ ) and size ( $D_{ice}$ ) of ice, together with the ambient supersaturation over ice ( $S_{ice}$ ). In our simulations, the averaged  $S_{ice}$  and  $D_{ice}$  are not sensitive to the aerosol disturbance; it is  $N_{ice}$  that has been increased significantly because of elevated aerosol concentrations. Higher  $N_{ice}$  provides a larger surface area for water vapor deposition on the existing ice crystals and increases  $R_{vdi}$ . Lee and Penner (2010) suggested similar mechanisms for cirrus clouds, based on the double-moment bulk representation of Saleeby and Cotton (2004).

The process of the formation and dissipation of frozen water content in the modeling area is illustrated in Fig. 21. The ice crystals form firstly at a higher height, followed by the snow production at a lower level. Downdrafts in the margin region are caused mainly by evaporation and melting. Massive melting takes place at the late stage (after 90 min), when large frozen particles (i.e., graupel) form. This is in agreement with the fact that the raindrops appear at a late stage and at a lower altitude under strong FF conditions (Fig. 8c and d).

As shown aforementioned, drop freezing parameterizations and ice nucleation parameterizations influence frozen water content dramatically, which involve large uncertainties. Ice microphysics are significantly more complicated due

to the wide variety of ice particle characteristics. On the one hand, the intensities of these processes differ greatly among different microphysical schemes. Eidhammer et al. (2009) compared three different ice nucleation parameterizations and found that different assumptions could result in similar qualitative conclusions although with distinct absolute values. The parameterization with observational constraints agrees well with the measurements. On the other hand, van Lier-Walqui et al. (2012) suggested the processes contributing to frozen particles are dependent on both particle size distribution and density parameters. Parameterization improvement based on observations could help to reduce the uncertainties.

### 3.3.4 Contribution of individual microphysical processes

ATHAM consists of tens of microphysical processes. However, based on the calculation of their relative contributions, only a few processes play dominant roles in regulating the number and mass concentrations of cloud hydrometeors, suggesting a possibility for the simplification of microphysical schemes.

For the number concentration of cloud droplets, the cloud nucleation (cn) and cfi (freezing of cloud droplets to form ice) processes contribute most to its budget, while other processes together account for less than 10%. For the mass concentration, the net change in vdc (condensational growth of cloud droplets by deposition) and cep (evaporation of cloud droplets) processes determines the variations in the cloud water content. The cfi process could contribute  $\sim 50\%$  of the sink under HULA conditions. Therefore, when we simulate the mass of cloud droplets, four microphysical processes, i.e., cn, vdc, cep, and cfi, account for a large fraction of the budget.

The dominant processes that contribute  $\sim 90\%$  to the raindrop number concentration under specific conditions are autoconversion (au); self-collection (rsc); evaporation (rep); and melting of ice, snow, and graupel (imr, smr, and gmr). For the raindrop mass concentration, the contribution of three processes accounts for  $\sim 90\%$  under most conditions, which are rain evaporation (rep) and melting of snow and graupel (smr, and gmr).

For the frozen water content, under weak fire forcing conditions, vdi (condensational growth of ice crystals by deposition) and sep (snow evaporation) contribute  $\sim 90\%$  of the source and sink, respectively. Under strong fire forcing conditions, vdi and cfi together contribute 90% of the source, while sep and gmr together are the most important sink (90%).

These major processes can capture most of the qualitative and quantitative features of pyro-convection processes and this complex model can thus be simplified for many purposes to improve the computational capacity. Comparison between

the comprehensive model and simplified framework will be performed and validated in future studies.

### 3.4 Uncertainties due to nonlinearity

Aerosol-cloud interactions are regarded as nonlinear processes. In this case, the local aerosol effects on a cloud-relevant parameter  $Y$ , i.e.,  $dY/dN_{\text{CN}}$ , can be different from  $\Delta Y/\Delta N_{\text{CN}}$ , with the dependence derived from two case studies. Figure 1 shows such an example: depending on the case selection, a positive (or negative)  $dY/dN_{\text{CN}}$  can correspond to a  $\Delta Y/\Delta N_{\text{CN}}$  of 0. The question then arises of how much difference can be expected between  $dY/dN_{\text{CN}}$  and  $\Delta Y/\Delta N_{\text{CN}}$ . In the following, we take the responses of the precipitation to aerosols as an example to address this issue.

Figure 22 shows the statistics of the relative difference between  $\Delta Y/\Delta N_{\text{CN}}$  and  $dY/dN_{\text{CN}}$  under LU and HU conditions, in which  $Y$  represents the precipitation rate. As precipitation is insensitive to aerosols for  $N_{\text{CN}} > 10\,000\text{ cm}^{-3}$ , only the cases with  $N_{\text{CN}}$  of  $200 \sim 10\,000\text{ cm}^{-3}$  are chosen in the calculation. The relative difference is defined as

$$\text{Relative difference} = \frac{\frac{\Delta Y}{\Delta N_{\text{CN}}} - \frac{dY}{dN_{\text{CN}}}}{\frac{dY}{dN_{\text{CN}}}}, \quad (2)$$

and  $\frac{\Delta Y}{\Delta N_{\text{CN}}}$  is calculated as  $\frac{\Delta Y}{\Delta N_{\text{CN}}} = \frac{Y(2N_{\text{CN}}) - Y(N_{\text{CN}})}{2N_{\text{CN}} - N_{\text{CN}}}$ , in which the aerosol effect is determined by the difference between the reference case and that after doubling  $N_{\text{CN}}$ .  $\frac{dY}{dN_{\text{CN}}}$  is the derivative of the precipitation rate at each  $N_{\text{CN}}$ , representing the local dependence of precipitation on  $N_{\text{CN}}$ .

The histograms in Fig. 22 demonstrate that  $\frac{\Delta Y}{\Delta N_{\text{CN}}}$  can deviate considerably from  $\frac{dY}{dN_{\text{CN}}}$ , not only for the absolute value but also for the sign. Statistically, most of the relative differences are in the range of  $-3.7 \sim 0.9$  (the 25th and 75th percentiles, respectively, with the average difference of  $-3.0$ ) under LU conditions, while they are between  $-1.5$  and  $0.04$  (the 25th and 75th percentiles, respectively, with the mean value of  $0.02$ ) under HU conditions. The fact that individual case studies may not reveal local aerosol effects demonstrates the importance of ensemble studies in determining the real responses of clouds to aerosol perturbations.

## 4 Conclusions

In this study, the regime dependence of aerosol effects on the formation and evolution of pyro-convective clouds has been studied in detail (Fig. 23). The main conclusions are summarized as follows:

1. As aerosol number concentration ( $N_{\text{CN}}$ ) and fire forcing (FF) increased, the number concentration of cloud droplets increased. There are three distinct regimes for the cloud number concentration: an updraft-limited regime (high relative sensitivity (RS) ratio of

$\text{RS(FF)}/\text{RS}(N_{\text{CN}})$ ), an aerosol-limited regime (low  $\text{RS(FF)}/\text{RS}(N_{\text{CN}})$  ratio), and a transitional regime (intermediate  $\text{RS(FF)}/\text{RS}(N_{\text{CN}})$  ratio). This agrees well with the regimes derived from a parcel model (Reutter et al., 2009). The cloud mass concentration is less sensitive to aerosols, and there are two regimes for mass concentration: an updraft-limited regime and a transitional regime.

2. The production of rain water content (i.e.,  $M_{\text{RD}}$ ) was enhanced with increase in updrafts, and the aerosols could either slightly increase  $M_{\text{RD}}$  with low aerosol concentration or decrease  $M_{\text{RD}}$  with large aerosol concentration. The aerosol concentration plays a mostly negative role in  $M_{\text{CD}}$  under intermediate aerosol conditions (aerosol number concentration of several  $1000\text{ cm}^{-3}$ ).  $M_{\text{RD}}$  was generally within an updraft-limited regime – i.e.,  $M_{\text{RD}}$  was very sensitive to changes in updrafts but insensitive to aerosol concentrations ( $\text{RS(FF)}/\text{RS}(N_{\text{CN}}) > 4$ ). The aerosol and updraft effects on raindrop number concentrations ( $N_{\text{RD}}$ ) are quite complicated; both of them play the non-monotonic role in the  $N_{\text{RD}}$ .
3. As updrafts and aerosols increased, the domain-averaged number and mass concentrations of frozen particles ( $N_{\text{FP}}$  and  $M_{\text{FP}}$ , respectively) were enhanced.  $N_{\text{FP}}$  and  $M_{\text{FP}}$  were also within the updraft-limited regime, which is characterized by large  $\text{RS(FF)}/\text{RS}(N_{\text{CN}})$  ratio. In this regime,  $N_{\text{FP}}$  and  $M_{\text{FP}}$  were directly proportional to fire forcing, and independent of aerosols.
4. Larger fire forcing resulted in more precipitation, whereas the effect of aerosols on precipitation was complex and could either enhance or suppress the production of precipitation. The suppression of the precipitation is due to the change in the fraction of small frozen particles and total melting rate of frozen particles. The enhancement on the precipitation resulting from increasing  $N_{\text{CN}}$  under low-aerosol conditions is a result of changes in the vertical distribution of frozen particles and its evaporation process.
5. In addition, when aerosol number concentration and fire forcing became too large, their impact became weaker, as indicated by a decreasing RS.

The process analysis (PA) provided further insight into the mechanisms of aerosol–cloud interactions. By evaluating the contribution of the relevant microphysical processes to the formation of an individual hydrometeor, the PA revealed the dominant factors responsible for the changes in hydrometeor number and mass. (1) Cloud nucleation (cn) initializes cloud droplet formation and is the major factor that controls the number concentration of cloud droplets. As expected, the increase in cloud droplet mass can be mostly attributed to

the condensational growth (vdc). (2) Under weak fire forcing conditions, autoconversion (au) and accretion (ac) are the main sources of rain droplets. Under strong fire forcing conditions, the major source is the melting of frozen particles. (3) For the frozen content, the condensation of water vapor on existing ice crystals (vdi) is the most important contributor. In addition to CCN activation, the PA also highlights the importance of other microphysical processes in regulating cloud evolution, which is worthy of further scrutiny. By identifying the contribution from individual processes, PA may also provide an opportunity for the simplification of microphysical schemes. For example, out of 24 microphysical processes that are directly related to the budget of cloud droplets and raindrops, over 90% of the mass and number changes are attributed to only 10 processes.

While the general trend is clear, the inclusion of nonlinear (dynamic and microphysical) processes leads to a complex and unstable response of clouds to aerosol perturbations. This applies to the response of all hydrometeors and precipitation, as indicated by the large standard deviation of relative sensitivities in Figs. 7, 9, 12, and 13. This should also hold when variations in other parameters (e.g., meteorological conditions) are introduced. Compared with our results, the relative sensitivities derived from cloud parcel modeling are much smoother (Fig. 8 in Reutter et al., 2009). The difference is probably caused by complex interactions between cloud microphysics and dynamics (Khain et al., 2008; Fan et al., 2009). These highly nonlinear processes result in a more unstable and chaotic response of cloud evolution to aerosol and dynamic perturbations. Because of this nonlinearity, sensitivities of clouds based on limited case studies may require caveats, because they may not be as representative as expected, and therefore cannot safely be extrapolated to conditions outside of the range explored. To better understand the role of aerosols in cloud formation, we recommend high-resolution ensemble sensitivity studies over a wide range of dynamic and aerosol conditions.

Current general understanding and global modeling studies suggest that, for cloud droplet number concentration, the updraft-limited regime may be more characteristic of continental clouds, while the aerosol-limited regime may be more characteristic of marine clouds (e.g., Karydis et al., 2012), suggesting that aerosol effects are generally more important for the marine environment. For this case study of pyro-convective clouds, then, we conclude that aerosol effects on cloud droplet number concentrations and cloud droplet size are likely more important than effects on precipitation, since precipitation is far less sensitive to aerosol number concentrations than to updraft velocity. This is in agreement with other studies (e.g., Seifert et al., 2012). A recent long-term convective cloud investigation found that microphysical effects driven by aerosol particles dominate the properties and morphology of deep convective clouds, rather than updraft-related dynamics (Fan et al., 2013). Therefore, whether this conclusion applies to other cloud types and over longer timescales still needs to be determined.

In this study, we demonstrate the performance of ensemble simulations in determining the regime dependence of aerosol effects. The use of such regime dependence requires caveats because it may differ for different cloud types, aerosol properties, meteorological conditions, and model configurations (e.g., microphysical schemes, dynamic schemes, and dimensionality; the 3-D results can be found in the Supplement).

In future work, we intend to extend the current studies to (1) include other types of clouds with other meteorological or atmospheric conditions; (2) investigate the cloud response over longer timescales (Van Den Heever and Cotton, 2007), as different observational scales could introduce biases into the quantification of aerosol effects on clouds (McComiskey and Feingold, 2012); and (3) evaluate the relative contribution of microphysical and dynamic effects to cloud buffering effects (Stevens and Feingold, 2009; Seifert et al., 2012).

## Appendix A

**Table A1.** Abbreviations and descriptions for individual microphysical process.

Abbreviation	Process
cn	Cloud nucleation
cri/s/g/h	Riming of cloud droplets to form ice crystals/snow/graupel/hail
cfi <sup>(1)</sup>	Freezing of cloud water to form ice crystals
imc/r	Melting of ice crystals to form cloud water/raindrops
au	Autoconversion of cloud water to form rain
ac	Accretion of cloud water by rain
vdc/i/g/s	Condensational growth of cloud droplets/ice crystals/graupel/snow by vapor deposition
in	Ice nucleation
s/g/hmr	Melting of snow/graupel/hail to form raindrops
rsc	Self-collection of raindrops
rfi/s/g/h	Freezing of raindrops to form ice crystals/snow/graupel/hail
rri/s/g/h	Riming of raindrops to form ice crystals/snow/graupel/hail
c/r/i/s/gep	Evaporation of cloud droplets/raindrops/ice/snow/graupel

<sup>1</sup> Here, cfi process includes both heterogeneous and homogeneous freezing processes.

The Supplement related to this article is available online at doi:10.5194/acp-15-10325-2015-supplement.

*Acknowledgements.* This work was supported by the Max Planck Society (MPG), Max Planck Graduate Center (MPGC), and EU project BACCHUS (no. 603445). S. M. Burrows was supported by the Office of Science Biological and Environmental Research Program of the US Department of Energy as part of the Earth System Modeling Program. We thank A. Seifert, and P. Neis for helpful discussions and model setup.

The article processing charges for this open-access publication were covered by the Max Planck Society.

Edited by: X. Liu

## References

- Ackerman, A. S., Toon, O. B., Stevens, D. E., Heymsfield, A. J., Ramanathan, V., and Welton, E. J.: Reduction of tropical cloudiness by soot, *Science*, 288, 1042–1047, doi:10.1126/science.288.5468.1042, 2000.
- Ackerman, A. S., Toon, O. B., Stevens, D. E., and Coakley, J. A.: Enhancement of cloud cover and suppression of nocturnal drizzle in stratocumulus polluted by haze, *Geophys. Res. Lett.*, 30, 1381, doi:10.1029/2002gl016634, 2003.
- Albrecht, B. A.: Aerosols, Cloud Microphysics, and Fractional Cloudiness, *Science*, 245, 1227–1230, doi:10.1126/science.245.4923.1227, 1989.
- Altartaz, O., Koren, I., Reisin, T., Kostinski, A., Feingold, G., Levin, Z., and Yin, Y.: Aerosols' influence on the interplay between condensation, evaporation and rain in warm cumulus cloud, *Atmos. Chem. Phys.*, 8, 15–24, doi:10.5194/acp-8-15-2008, 2008.
- Andreae, M. O., Rosenfeld, D., Artaxo, P., Costa, A. A., Frank, G. P., Longo, K. M., and Silva-Dias, M. A. F.: Smoking Rain Clouds over the Amazon, *Science*, 303, 1337–1342, 2004.
- ASRD: Final Documentation Report – Chisholm Fire (LWF-063), Forest Protection Division, ISBN 0-7785-1841-8, Tech. rep., Alberta Sustainable Resource Development, 2001.
- Blahak, U.: Towards a Better Representation of High Density Ice Particles in a State-of-the-Art Two-Moment Bulk Microphysical Scheme, 15th International Conf. on Clouds and Precipitation, Cancun, Mexico, 7–11 July, 2008.
- Bytnerowicz, A., Arbaugh, M., Andersen, C., and Riebau, A.: Wildland Fires and Air Pollution, *Dev. Environm. Sci.*, 8, 1–638, 2009.
- Camponogara, G., Dias, M. A. F. S., and Carrio, G. G.: Relationship between Amazon biomass burning aerosols and rainfall over the La Plata Basin, *Atmos. Chem. Phys.*, 14, 4397–4407, doi:10.5194/acp-14-4397-2014, 2014.
- Cotton, R. J. and Field, P. R.: Ice nucleation characteristics of an isolated wave cloud, *Q. J. Roy. Meteor. Soc.*, 128, 2417–2437, doi:10.1256/Qj.01.150, 2002.
- Eidhammer, T., DeMott, P. J., and Kreidenweis, S. M.: A comparison of heterogeneous ice nucleation parameterization using a parcel model framework, *J. Geophys. Res.*, 114, D06202, doi:10.1029/2008JD011095, 2009.
- Fan, J. W., Yuan, T. L., Comstock, J. M., Ghan, S., Khain, A., Leung, L. R., Li, Z. Q., Martins, V. J., and Ovchinnikov, M.: Dominant role by vertical wind shear in regulating aerosol effects on deep convective clouds, *J. Geophys. Res.-Atmos.*, 114, D22206, doi:10.1029/2009jd012352, 2009.
- Fan, J. W., Leung, L. R., Rosenfeld, D., Chen, Q., Li, Z. Q., Zhang, J. Q., and Yan, H. R.: Microphysical effects determine macrophysical response for aerosol impacts on deep convective clouds, *P. Natl. Acad. Sci. USA*, 110, E4581–E4590, doi:10.1073/pnas.1316830110, 2013.
- Feingold, G.: Modeling of the first indirect effect: Analysis of measurement requirements, *Geophys. Res. Lett.*, 30, 1997, doi:10.1029/2003GL017967, 2003.
- Graf, H. F., Herzog, M., Oberhuber, J. M., and Textor, C.: Effect of environmental conditions on volcanic plume rise, *J. Geophys. Res.-Atmos.*, 104, 24309–24320, 1999.
- Grandey, B. S., Stier, P., and Wagner, T. M.: Investigating relationships between aerosol optical depth and cloud fraction using satellite, aerosol reanalysis and general circulation model data, *Atmos. Chem. Phys.*, 13, 3177–3184, doi:10.5194/acp-13-3177-2013, 2013.
- Herzog, M.: Simulation der dynamik eines multikomponentensystems am beispiel vulkanischer eruptionswolken, Ph. D, University of Hamburg, Hamburg, Germany, 153 pp., 1998.
- Herzog, M., Graf, H. F., Textor, C., and Oberhuber, J. M.: The effect of phase changes of water on the development of volcanic plumes, *J. Volcanol. Geoth. Res.*, 87, 55–74, 1998.
- Herzog, M., Oberhuber, J. M., and Graf, H. F.: A prognostic turbulence scheme for the nonhydrostatic plume model ATHAM, *J. Atmos. Sci.*, 60, 2783–2796, 2003.
- Hobbs, P. V. and Locatelli, J. D.: Ice nuclei from a natural forest fire, *J. Appl. Meteorol.*, 8, 833–834, 1969.
- Hobbs, P. V. and Radke, L. F.: Cloud Condensation Nuclei from a Simulated Forest Fire, *Science*, 163, 279–280, 1969.
- IPCC: Climate change 2007: The physical science basis, Contribution of Working Group I to the Fourth Assessment Report of the Intergovernmental Panel on Climate Change, edited by: Solomon, S., Qin, D., Manning, M., Chen, Z., Marquis, M., Averyt, K. B., Tignor, M., and Miller, H. L., Cambridge University Press, Cambridge and New York, 996 pp., 2007.
- Jayaweera, K. and Ryan, B. F.: Terminal Velocities of Ice Crystals, *Q. J. Roy. Meteor. Soc.*, 98, 193–197, doi:10.1002/qj.49709841516, 1972.
- Jeffery, C. A. and Austin, P. H.: Homogeneous nucleation of supercooled water: Results from a new equation of state, *J. Geophys. Res.-Atmos.*, 102, 25269–25279, doi:10.1029/97jd02243, 1997.
- Karydis, V. A., Capps, S. L., Russell, A. G., and Nenes, A.: Adjoint sensitivity of global cloud droplet number to aerosol and dynamical parameters, *Atmos. Chem. Phys.*, 12, 9041–9055, doi:10.5194/acp-12-9041-2012, 2012.
- Kaufman, Y. J. and Fraser, R. S.: The effect of smoke particles on clouds and climate forcing, *Science*, 277, 1636–1639, 1997.
- Kaufman, Y. J. and Koren, I.: Smoke and pollution aerosol effect on cloud cover, *Science*, 313, 655–658, doi:10.1126/science.1126232, 2006.

- Kaufman, Y. J., Tanre, D., and Boucher, O.: A satellite view of aerosols in the climate system, *Nature*, 419, 215–223, doi:10.1038/Nature01091, 2002.
- Kay, J. E. and Wood, R.: Timescale analysis of aerosol sensitivity during homogeneous freezing and implications for upper tropospheric water vapor budgets, *Geophys. Res. Lett.*, 35, L10809, doi:10.1029/2007gl032628, 2008.
- Khain, A., Rosenfeld, D., and Pokrovsky, A.: Aerosol impact on the dynamics and microphysics of deep convective clouds, *Q. J. Roy. Meteor. Soc.*, 131, 2639–2663, doi:10.1256/Qj.04.62, 2005.
- Khain, A. P.: Notes on state-of-the-art investigations of aerosol effects on precipitation: a critical review, *Environ Res Lett*, 4, doi:10.1088/1748-9326/4/1/015004, 2009.
- Khain, A. P., BenMoshe, N., and Pokrovsky, A.: Factors determining the impact of aerosols on surface precipitation from clouds: An attempt at classification, *J. Atmos. Sci.*, 65, 1721–1748, doi:10.1175/2007jas2515.1, 2008.
- Khain, A. P., Leung, L. R., Lynn, B., and Ghan, S.: Effects of aerosols on the dynamics and microphysics of squall lines simulated by spectral bin and bulk parameterization schemes, *J. Geophys. Res.-Atmos.*, 114, D22203, doi:10.1029/2009jd011902, 2009.
- Kohler, H.: The nucleus in and the growth of hygroscopic droplets, *Trans. Faraday Soc.*, 32, 1152–1161, doi:10.1039/Tf9363201152, 1936.
- Koren, I., Kaufman, Y. J., Remer, L. A., and Martins, J. V.: Measurement of the effect of Amazon smoke on inhibition of cloud formation, *Science*, 303, 1342–1345, doi:10.1126/science.1089424, 2004.
- Kulmala, M., Laaksonen, A., Charlson, R. J., and Korhonen, P.: Clouds without supersaturation, *Nature*, 388, 336–337, doi:10.1038/41000, 1997.
- Laaksonen, A., Korhonen, P., Kulmala, M., and Charlson, R. J.: Modification of the Kohler equation to include soluble trace gases and slightly soluble substances, *J. Atmos. Sci.*, 55, 853–862, 1998.
- Lee, S. S. and Penner, J. E.: Aerosol effects on ice clouds: can the traditional concept of aerosol indirect effects be applied to aerosol-cloud interactions in cirrus clouds?, *Atmos. Chem. Phys.*, 10, 10345–10358, doi:10.5194/acp-10-10345-2010, 2010.
- Lee, S. S. and Feingold, G.: Aerosol effects on the cloud-field properties of tropical convective clouds, *Atmos. Chem. Phys.*, 13, 6713–6726, doi:10.5194/acp-13-6713-2013, 2013.
- Lee, S. S., Donner, L. J., Phillips, V. T. J., and Ming, Y.: The dependence of aerosol effects on clouds and precipitation on cloud-system organization, shear and stability, *J. Geophys. Res.-Atmos.*, 113, D16202, doi:10.1029/2007jd009224, 2008.
- Levin, Z. and Cotton, W.: *Aerosol Pollution Impact on Precipitation: A Scientific Review*, World Meteorol. Organ, Geneva, Switzerland, 2007.
- Li, G. H., Wang, Y., and Zhang, R. Y.: Implementation of a two-moment bulk microphysics scheme to the WRF model to investigate aerosol-cloud interaction, *J. Geophys. Res.-Atmos.*, 113, D15211, doi:10.1029/2007jd009361, 2008.
- Luderer, G. G.: *Modeling of Deep-Convective Vertical Transport of Forest Fire Smoke into the Upper Troposphere and Lower Stratosphere*, Ph.D, Physics Department, Johannes Gutenberg University Mainz, Mainz, 2007.
- McComiskey, A. and Feingold, G.: The scale problem in quantifying aerosol indirect effects, *Atmos. Chem. Phys.*, 12, 1031–1049, doi:10.5194/acp-12-1031-2012, 2012.
- McFiggans, G., Artaxo, P., Baltensperger, U., Coe, H., Facchini, M. C., Feingold, G., Fuzzi, S., Gysel, M., Laaksonen, A., Lohmann, U., Mentel, T. F., Murphy, D. M., O'Dowd, C. D., Snider, J. R., and Weingartner, E.: The effect of physical and chemical aerosol properties on warm cloud droplet activation, *Atmos. Chem. Phys.*, 6, 2593–2649, doi:10.5194/acp-6-2593-2006, 2006.
- Mitchell, D. L. and Heymsfield, A. J.: Refinements in the treatment of ice particle terminal velocities, highlighting aggregates, *J. Atmos. Sci.*, 62, 1637–1644, doi:10.1175/Jas3413.1, 2005.
- Muhlbauer, A., Hashino, T., Xue, L., Teller, A., Lohmann, U., Rasmussen, R. M., Geresdi, I., and Pan, Z.: Intercomparison of aerosol-cloud-precipitation interactions in stratiform orographic mixed-phase clouds, *Atmos. Chem. Phys.*, 10, 8173–8196, doi:10.5194/acp-10-8173-2010, 2010.
- Norris, J. R.: Has northern Indian Ocean cloud cover changed due to increasing anthropogenic aerosol?, *Geophys. Res. Lett.*, 28, 3271–3274, doi:10.1029/2001gl013547, 2001.
- Oberhuber, J. M., Herzog, M., Graf, H. F., and Schwanke, K.: Volcanic plume simulation on large scales, *J. Volcanol. Geoth. Res.*, 87, 29–53, 1998.
- Pruppacher, H. R. and Klett, J. D.: *Microphysics of Clouds and Precipitation*, Second Revised and Enlarged Edition with an Introduction to Cloud Chemistry and Cloud Electricity, Kluwer Academic Publishers, Reidel, Dordrecht, 954 pp., 1997.
- Reid, J. S., Koppmann, R., Eck, T. F., and Eleuterio, D. P.: A review of biomass burning emissions part II: intensive physical properties of biomass burning particles, *Atmos. Chem. Phys.*, 5, 799–825, doi:10.5194/acp-5-799-2005, 2005.
- Reutter, P., Su, H., Trentmann, J., Simmel, M., Rose, D., Gunthe, S. S., Wernli, H., Andreae, M. O., and Pöschl, U.: Aerosol- and updraft-limited regimes of cloud droplet formation: influence of particle number, size and hygroscopicity on the activation of cloud condensation nuclei (CCN), *Atmos. Chem. Phys.*, 9, 7067–7080, doi:10.5194/acp-9-7067-2009, 2009.
- Reutter, P., Trentmann, J., Seifert, A., Neis, P., Su, H., Chang, D., Herzog, M., Wernli, H., Andreae, M. O., and Pöschl, U.: 3-D model simulations of dynamical and microphysical interactions in pyro-convective clouds under idealized conditions, *Atmos. Chem. Phys.*, 14, 7573–7583, doi:10.5194/acp-14-7573-2014, 2014.
- Rosenfeld, D.: TRMM observed first direct evidence of smoke from forest fires inhibiting rainfall, *Geophys. Res. Lett.*, 26, 3105–3108, 1999.
- Rosenfeld, D.: Suppression of rain and snow by urban and industrial air pollution, *Science*, 287, 1793–1796, 2000.
- Rosenfeld, D., Fromm, M., Trentmann, J., Luderer, G., Andreae, M. O., and Servranckx, R.: The Chisholm firestorm: observed microstructure, precipitation and lightning activity of a pyro-cumulonimbus, *Atmos. Chem. Phys.*, 7, 645–659, doi:10.5194/acp-7-645-2007, 2007.
- Rosenfeld, D., Lohmann, U., Raga, G. B., O'Dowd, C. D., Kulmala, M., Fuzzi, S., Reissell, A., and Andreae, M. O.: Flood or drought: How do aerosols affect precipitation?, *Science*, 321, 1309–1313, doi:10.1126/science.1160606, 2008.
- Saleeby, S. M. and Cotton, W. R.: A large-droplet mode and prognostic number concentration of cloud droplets in the Col-

- orado State University Regional Atmospheric Modeling System (RAMS). Part I: Module descriptions and supercell test simulations, *J. Appl. Meteorol.*, 43, 182–195, doi:10.1175/1520-0450(2004)043, 2004.
- Saleeby, S. M., Cotton, W. R., Lowenthal, D., Borys, R. D., and Wetzel, M. A.: Influence of Cloud Condensation Nuclei on Orographic Snowfall, *J. Appl. Meteorol. Clim*, 48, 903–922, doi:10.1175/2008jamc1989.1, 2009.
- Sassen, K. and Khvorostyanov, V. I.: Cloud effects from boreal forest fire smoke: evidence for ice nucleation from polarization lidar data and cloud model simulations, *Environ. Res. Lett.*, 3, 025006, doi:10.1088/1748-9326/3/2/025006, 2008.
- Seifert, A. and Beheng, K. D.: A two-moment cloud microphysics parameterization for mixed-phase clouds. Part I: Model description, *Meteorol. Atmos. Phys.*, 92, 45–66, doi:10.1007/s00703-005-0112-4, 2006.
- Seifert, A., Khain, A., Pokrovsky, A., and Beheng, K. D.: A comparison of spectral bin and two-moment bulk mixed-phase cloud microphysics, *Atmos. Res.*, 80, 46–66, doi:10.1016/j.atmosres.2005.06.009, 2006.
- Seifert, A., Kohler, C., and Beheng, K. D.: Aerosol-cloud-precipitation effects over Germany as simulated by a convective-scale numerical weather prediction model, *Atmos. Chem. Phys.*, 12, 709–725, doi:10.5194/acp-12-709-2012, 2012.
- Shulman, M. L., Jacobson, M. C., Charlson, R. J., Synovec, R. E., and Young, T. E.: Dissolution behavior and surface tension effects of organic compounds in nucleating cloud droplets, *Geophys. Res. Lett.*, 23, 603–603, doi:10.1029/96gl00594, 1996.
- Sorooshian, A., Feingold, G., Lebsock, M. D., Jiang, H. L., and Stephens, G. L.: On the precipitation susceptibility of clouds to aerosol perturbations, *Geophys. Res. Lett.*, 36, L13803, doi:10.1029/2009gl038993, 2009.
- Stevens, B. and Seifert, A.: Understanding macrophysical outcomes of microphysical choices in simulations of shallow cumulus convection, *J. Meteorol. Soc. Jpn.*, 86, 143–162, 2008.
- Stevens, B. and Feingold, G.: Untangling aerosol effects on clouds and precipitation in a buffered system, *Nature*, 461, 607–613, doi:10.1038/Nature08281, 2009.
- Tao, W. K., Li, X. W., Khain, A., Matsui, T., Lang, S., and Simpson, J.: Role of atmospheric aerosol concentration on deep convective precipitation: Cloud-resolving model simulations, *J. Geophys. Res.-Atmos.*, 112, D24S18, doi:10.1029/2007jd008728, 2007.
- Tao, W. K., Chen, J. P., Li, Z. Q., Wang, C., and Zhang, C. D.: Impact of Aerosols on Convective Clouds and Precipitation, *Rev. Geophys.*, 50, RG2001, doi:10.1029/2011rg000369, 2012.
- Teller, A. and Levin, Z.: Factorial method as a tool for estimating the relative contribution to precipitation of cloud microphysical processes and environmental conditions: Method and application, *J. Geophys. Res.-Atmos.*, 113, D02202, doi:10.1029/2007jd008960, 2008.
- Van Den Heever, S. C. and Cotton, W. R.: Urban aerosol impacts on downwind convective storms, *J. Appl. Meteorol. Clim*, 46, 828–850, doi:10.1175/Jam2492.1, 2007.
- van Lier-Walqui, M., Vukicevic, T., and Posselt, D. J.: Quantification of Cloud Microphysical Parameterization Uncertainty Using Radar Reflectivity, *Mon. Weather Rev.*, 140, 3442–3466, doi:10.1175/Mwr-D-11-00216.1, 2012.
- Wang, Y., Wan, Q., Meng, W., Liao, F., Tan, H., and Zhang, R.: Long-term impacts of aerosols on precipitation and lightning over the Pearl River Delta megacity area in China, *Atmos. Chem. Phys.*, 11, 12421–12436, 10, <http://www.atmos-chem-phys.net/11/12421/10/5194/acp-11-12421-2011>, 2011.
- Wang, Y., Fan, J. W., Zhang, R. Y., Leung, L. R., and Franklin, C.: Improving bulk microphysics parameterizations in simulations of aerosol effects, *J. Geophys. Res.-Atmos.*, 118, 5361–5379, doi:10.1002/Jgrd.50432, 2013.
- Wang, Y., Zhang, R. Y., and Saravanan, R.: Asian pollution climatically modulates mid-latitude cyclones following hierarchical modelling and observational analysis, *Nat. Commun.*, 5, 3098, doi:10.1038/Ncomms4098, 2014.
- Wood, R.: Drizzle in stratiform boundary layer clouds. Part II: Microphysical aspects, *J. Atmos. Sci.*, 62, 3034–3050, doi:10.1175/Jas3530.1, 2005.
- Yin, Y., Carslaw, K. S., and Feingold, G.: Vertical transport and processing of aerosols in a mixed-phase convective cloud and the feedback on cloud development, *Q. J. Roy. Meteor. Soc.*, 131, 221–245, doi:10.1256/qj.03.186, 2005.
- Zhang, L. M., Michelangeli, D. V., and Taylor, P. A.: Influence of aerosol concentration on precipitation formation in low-level, warm stratiform clouds, *J. Aerosol. Sci.*, 37, 203–217, doi:10.1016/j.jaerosci.2005.04.002, 2006.